12-21-2015

Enriched continental flood basalts from depleted mantle melts: modeling the lithospheric contamination of Karoo lavas from Antarctica

Jussi S. Heinonen

Arto V. Luttinen

Wendy A. Bohrson

Heinonen, J.S., Luttinen, A.V., Bohrson, W.A. 2016. Enriched continental flood basalts from depleted mantle melts: modeling the lithospheric contamination of Karoo lavas from Antarctica. Contributions to Mineralogy and Petrology 171:9. http://dx.doi.org/10.1007/s00410-015-1214-8
(Author's postprint)

Enriched continental flood basalts from depleted mantle melts: modeling the lithospheric contamination of Karoo lavas from Antarctica

Jussi S. Heinonen[1,2*], Arto V. Luttinen[2], Wendy A. Bohrson[3]
*[1]Department of Geosciences and Geography, University of Helsinki, P.O. Box 64, 00014 Helsinki, Finland (*corresponding author: jussi.s.heinonen@helsinki.fi, tel. +358 50 3185304)*
[2]Finnish Museum of Natural History, University of Helsinki, P.O. Box 44, 00014 Helsinki, Finland
[3]Department of Geological Sciences, Central Washington University, Ellensburg, WA 98926, USA

Abstract
Continental flood basalts (CFBs) represent large-scale melting events in the Earth's upper mantle and show considerable geochemical heterogeneity that is typically linked to substantial contribution from underlying continental lithosphere. Large-scale partial melting of the cold subcontinental lithospheric mantle and the large amounts of crustal contamination suggested by traditional binary mixing or assimilation-fractional crystallization models are difficult to reconcile with the thermal and compositional characteristics of continental lithosphere, however. The well-exposed CFBs of Vestfjella, western Dronning Maud Land, Antarctica, belong to the Jurassic Karoo large igneous province and provide a prime locality to quantify mass contributions of lithospheric and sublithospheric sources for two reasons: 1) recently discovered CFB dikes show isotopic characteristics akin to mid-ocean ridge basalts, and thus help to constrain asthenospheric parental melt compositions, and 2) the well-exposed basaltic lavas have been divided into four different geochemical magma types that exhibit considerable trace element and radiogenic isotope heterogeneity (e.g., initial ε_{Nd} from -16 to +2 at 180 Ma). We simulate the geochemical evolution of Vestfjella CFBs using 1) energy-constrained assimilation-fractional crystallization equations that account for heating and partial melting of crustal wallrock and 2) assimilation-fractional crystallization equations for lithospheric mantle contamination by using highly alkaline continental volcanic rocks (i.e. partial melts of mantle lithosphere) as contaminants. Calculations indicate that the different magma types can be produced by just minor (1–15 wt. %) contamination of asthenospheric parental magmas by melts from variable lithospheric reservoirs. Our models imply that the role of continental lithosphere as a CFB source component or contaminant may have been overestimated in many cases. Thus, CFBs may represent major juvenile crustal growth events rather than just recycling of old lithospheric materials.

Keywords: continental flood basalts; modeling; petrology; geochemistry; contamination; thermodynamics

Heinonen, J.S., Luttinen, A.V., Bohrson, W.A. 2016. Enriched continental flood basalts from depleted mantle melts: modeling the lithospheric contamination of Karoo lavas from Antarctica. Contributions to Mineralogy and Petrology 171:9. http://dx.doi.org/10.1007/s00410-015-1214-8
(Author's postprint)

Introduction

The massive outpourings of flood basalts represent very large-scale planetary melting events often attributed to thermal anomalies in the convective upper mantle. They are frequently linked to the opening of new ocean basins and have contributed to global climate change and extinctions of terrestrial and marine life (e.g., Black et al. 2014; Ganino and Arndt 2009).

The origin of continental flood basalt (CFB) provinces is controversial. Most CFBs do not represent primary melts, but have differentiated in large magma chambers within the lithosphere (e.g., Cox 1980; Farnetani et al. 1996). They generally exhibit strong geochemical affinities to continental rock types and many studies favor significant contributions from geochemically enriched subcontinental lithospheric mantle (SCLM; e.g., Lightfoot et al. 1993; Gibson et al. 1995; Jourdan et al. 2007a; Xu et al. 2007). In addition, the widely-used assimilation-fractional crystallization (AFC; e.g., DePaolo 1981b) models typically require high degrees (up to 60 wt. %) of (subsequent) crustal contamination to explain the most extreme enrichments in incompatible trace element and isotopic compositions (e.g., Carlson et al. 1981; Arndt et al. 1993; Molzahn et al. 1996; Ewart et al. 1998; Larsen and Pedersen 2009). Both of these scenarios are problematic, however. First, the capability of the cold, dry, and infertile (dominantly harzburgitic) cratonic SCLM to produce large quantities of melt is questionable (e.g., Arndt and Christensen 1992; Menzies 1992; Arndt et al. 1993) and would require that the SCLM is extensively hydrated (Gallagher and Hawkesworth 1992) and/or metasomatized (Harry and Leeman 1995). Second, high amounts of contamination with Si-rich crustal materials would result in silica-rich magma compositions not shown by the CFBs, and would require amounts of latent heat energy much greater than what is likely to be available (Spera and Bohrson 2001).

The parental melt compositions in many of the lithosphere-dominated CFB models are not well constrained. In addition, no allowance is generally made for progressive partial melting of crustal wallrock, despite excellent documentation of partial melting processes at the contacts of mafic intrusive rocks (e.g., Johnson et al. 2003; Hersum et al. 2007). Instead, most crustal contamination models mix a compositionally fixed bulk contaminant into a fractionating magma. These limitations may significantly impact the mass balance of lithospheric and sublithospheric sources in the generation of CFBs.

Energy-constrained AFC (EC-AFC) equations that account for energy and mass exchange between magma and wallrock (Bohrson and Spera 2001, 2003; Spera and Bohrson 2001, 2002, 2004), permit quantitative evaluation of the role of continental crust in CFB magma genesis. They account for energy and mass exchange in a system, in which a crystallizing magma body heats and partially melts crustal wallrock. In the case of contamination with SCLM, the poor knowledge of its bulk composition and thermodynamic parameters (e.g., solidus temperature) limits the applicability of EC-AFC equations. Partial melting of fertile SCLM can be mimicked, however, by using alkaline and ultrapotassic rocks (i.e. low-degree melts of metasomatized SCLM) as contaminants using traditional binary mixing or AFC equations (e.g., Ellam and Cox 1991; Hergt et al. 1991; Riley et al., 2005; Jourdan et al. 2007a).

The Karoo CFBs (Fig. 1) exposed at Vestfjella mountain range in western Dronning Maud Land, Antarctica (Fig. 2a), are ideal candidates for contamination modeling for two reasons. First, a group of basaltic dikes described from the area have Sr, Nd, Pb, and Os isotopic compositions akin to those of Southwest Indian Ridge mid-ocean ridge basalts (SWIR MORBs), and have been derived from depleted mantle (DM) sources at high pressures beneath the

Gondwanan lithosphere (Fig. 3; Luttinen and Furnes 2000; Heinonen et al. 2010; Luttinen et al. 2015). These dikes are rare but provide invaluable insight into the compositions of CFB magmas not influenced by the lithosphere, and therefore provide compositional estimates of uncontaminated, asthenosphere-derived parental magmas. Second, the detailed mapping of the well-exposed Vestfjella CFBs (~flow-by-flow sampling of ~1 km thick succession) have revealed four distinct CFB magma types that show a wide range of lithosphere-affinity trace element and isotopic compositions ($\varepsilon_{Nd(t)}$[1] from -16 to +2; Luttinen et al. 1998; Luttinen and Furnes 2000) nearly representing the whole degree of variation shown by the Karoo CFBs (Figs. 3b and 4). Previously presented AFC models implied that large crustal contributions (>20 wt. %) are needed to explain the most enriched geochemical signatures, and favored distinct parental magmas and mantle sources for the dominant magma types (Luttinen et al. 1998; Luttinen and Furnes 2000).

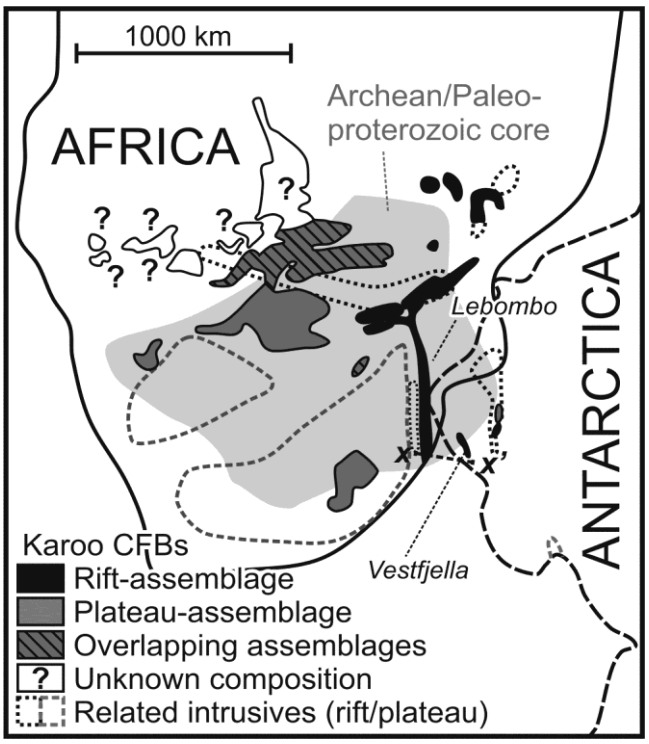

Fig. 1. Reconstruction of Africa and Antarctica at 180 Ma showing the present-day distribution of Karoo CFBs and related intrusive rocks (Luttinen and Siivola 1997; Jourdan et al. 2007b) and the Archean/Paleoproterozoic core complex of Kalahari (Jacobs et al. 2008). The line segment x–x' marks the approximate location of the schematic cross-section presented in Fig. 2b. Division into rift- and plateau-assemblage CFBs after Luttinen et al. (2015).

Our aim is to re-examine whether the exceptionally wide range of compositions described from enriched Karoo CFBs of Vestfjella can be explained by diversification of broadly uniform DM-sourced primary magmas due to contamination. We tackle this issue using quantitative EC-AFC and AFC modeling. The compositionally variable crustal rocks of the area and SCLM-

[1] Here, and hereafter, $\varepsilon_{Nd(t)}$ refers to the value calculated at 180 Ma, unless otherwise mentioned

derived alkaline and ultrapotassic rocks are used as contaminants. Our findings have important implications on the generation of CFBs and their geochemical characteristics.

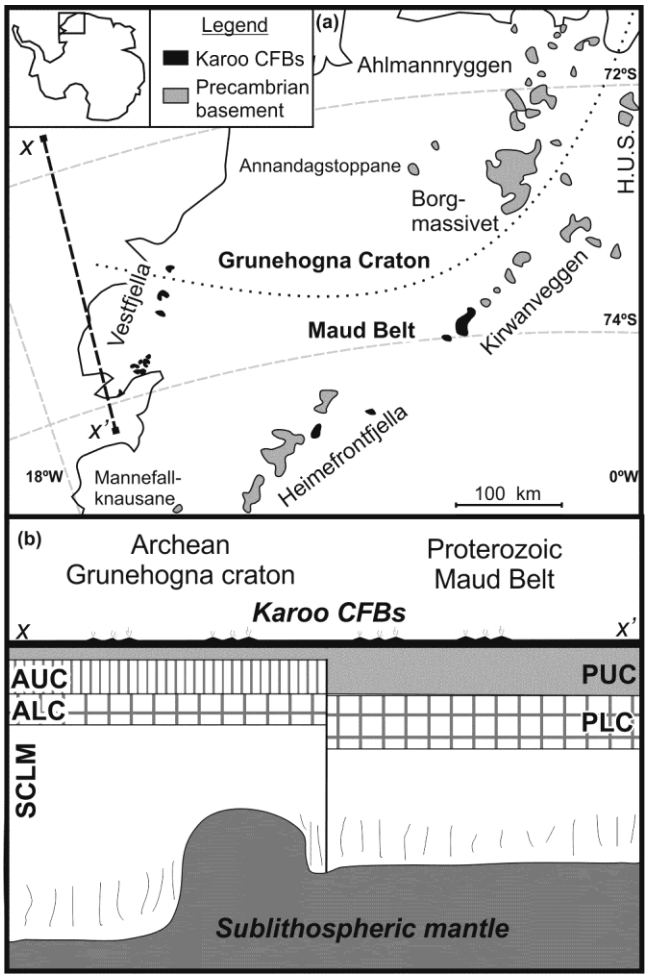

Fig. 2. (a) Distribution of Jurassic CFBs in western Dronning Maud Land. Lithospheric boundary reconstructed after Corner (1994). H.U.S. = H.U. Sverdrupfjella. (b) A schematic cross-section across line segment x–x' (Fig. 1 and 2a) during Karoo magmatism. AUC = Archean upper crust; ALC = Archean lower crust; PUC = Proterozoic upper crust; PLC = Proterozoic lower crust; SCLM = Subcontinental lithospheric mantle with metasomatized (veined) portions. Permian sedimentary rocks are known to exist between the Karoo CFBs and the Precambrian basement, but they are not shown in the cross-section.

Geological setting

The Karoo CFBs were generated during the initial stages of the breakup of the Gondwana supercontinent at ~190–180 Ma ago (e.g., Jourdan et al. 2005; Luttinen et al. 2015). The majority of the CFBs erupted in the continental interior of present-day southern Africa, but their remnants are also found in western Dronning Maud Land, Antarctica (Fig. 1).

The Karoo CFBs have highly heterogeneous trace element and isotopic compositions (e.g., $\varepsilon_{Nd(t)}$ from -16 to +3; Fig. 3b) generally ascribed to significant contribution from the underlying Precambrian basement and SCLM (e.g., Ellam 2006; Ellam and Cox 1989, 1991;

Harris et al. 1990; Hawkesworth et al. 1984; Jourdan et al. 2007a; Luttinen and Furnes 2000; Luttinen et al. 1998, Sweeney et al. 1991, 1994; Neumann et al. 2011). They have traditionally been divided into low-Ti and high-Ti provinces (e.g., Cox 1988; Sweeney et al. 1994), but the geochemical and geochronological data are more compatible with a division into 1) ~182 Ma *plateau-assemblage* CFBs composed of relatively monotonous and widespread low-Ti tholeiites and 2) ~190–174 Ma *rift-assemblage* CFBs composed of diverse low-Ti and high-Ti basalts and picrites sandwiched between nephelinites and felsic volcanic rocks in the main triple rift (Fig. 1; Luttinen et al. 2010, 2015). Comparison of incompatible element and isotopic compositions (Fig 3b) of these two sub-provinces indicates development in distinct magmatic systems (Luttinen et al. 2010, 2015).

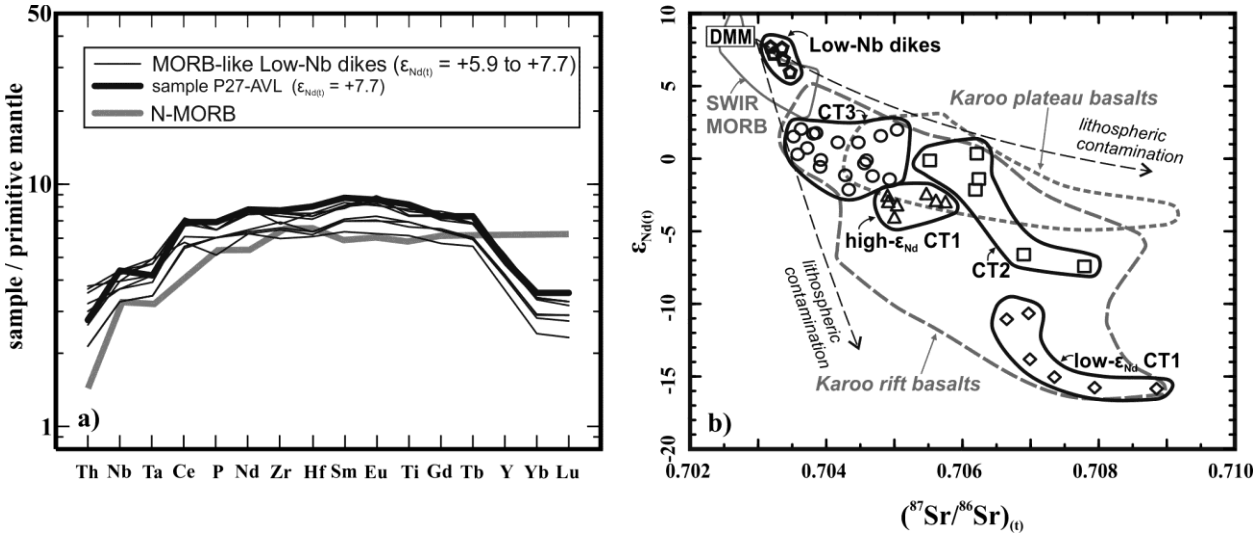

Fig. 3. a) Primitive-mantle-normalized (Sun and McDonough 1989) incompatible trace element patterns shown for the uncontaminated MORB-like Low-Nb dikes (n = 9; highlighting sample P27-AVL that is used to reconstruct the parental melt compositions; Luttinen and Furnes 2000; Heinonen et al. 2010) and average N-MORB (Sun and McDonough 1989). Note the effect of residual garnet (present at high pressures beneath the thick continental lithosphere) in the mantle source, responsible for the relatively lower Y, Yb, and Lu concentrations in the Low-Nb dikes relative to average MORB. b) Initial Sr and Nd isotopic characteristics of the Vestfjella lavas and Low-Nb dikes (Luttinen et al. 1998, 2015; Luttinen and Furnes 2000). "Lithosphere-signatured" Karoo rift- and plateau-assemblage CFBs (Hawkesworth et al. 1984; Ellam and Cox 1989, 1991; Harris et al. 1990; Sweeney et al. 1994; Riley et al. 2005, 2006; Jourdan et al. 2007a; Luttinen et al. 2010; Neumann et al. 2011), SWIR MORB (le Roex et al. 1983, 1992; Mahoney et al. 1992), and depleted MORB mantle (DMM; Workman and Hart 2005) also presented. The isotopic compositions of SWIR MORB sources and DMM were back-calculated at 180 Ma using DMM isotopic ratios after Workman and Hart (2005). Tentative lithospheric contamination trends after Heinonen et al. (2010).

The Antarctic Karoo CFBs are found in Vestfjella, Heimefrontfjella, and Kirwanveggen mountain ranges of western Dronning Maud Land, Antarctica (Fig. 2a). The CFBs are crosscut by related intrusive rocks that are additionally found crosscutting the Precambrian basement at Ahlmannryggen, Borgmassivet, H.U. Sverdrupfjella, and Mannefallknausane (Fig. 2a). The CFBs are underlain by Permian sedimentary rocks (e.g., Lindström 1995) and a heterogeneous Precambrian basement complex, which consists of two major units (Fig. 2): the Archean Grunehogna craton and the Mesoproterozoic Maud Belt that are related to the Kaapvaal craton

and the Namaqua-Natal metamorphic belts in southern Africa, respectively (Jacobs et al. 1993, 1998, 2003, 2008; Groenewald et al. 1995). The ≥ 3 Ga Grunehogna craton is exposed only in Annandagstoppane (Marschall et al. 2010) and is largely overlain by ~1100 Ma Ritscherflya sedimentary-volcanogenic rocks and intrusive ~1000 Ma Borgmassivet dikes and sills (e.g., Moyes et al. 1995). The Maud Belt is predominantly composed of high-grade metamorphic gneisses formed in the reworking of volcanic arc successions during the Grenvillean age orogeny ~1100 Ma ago (e.g., Groenewald et al. 1995; Grosch et al. 2007; Jacobs et al. 2003). Subsequent reworking during the Pan-African orogeny at ~600–500 Ma resulted in variable degree of magmatic and metamorphic overprinting of the Maud Belt (Jacobs et al. 1998, 2003).

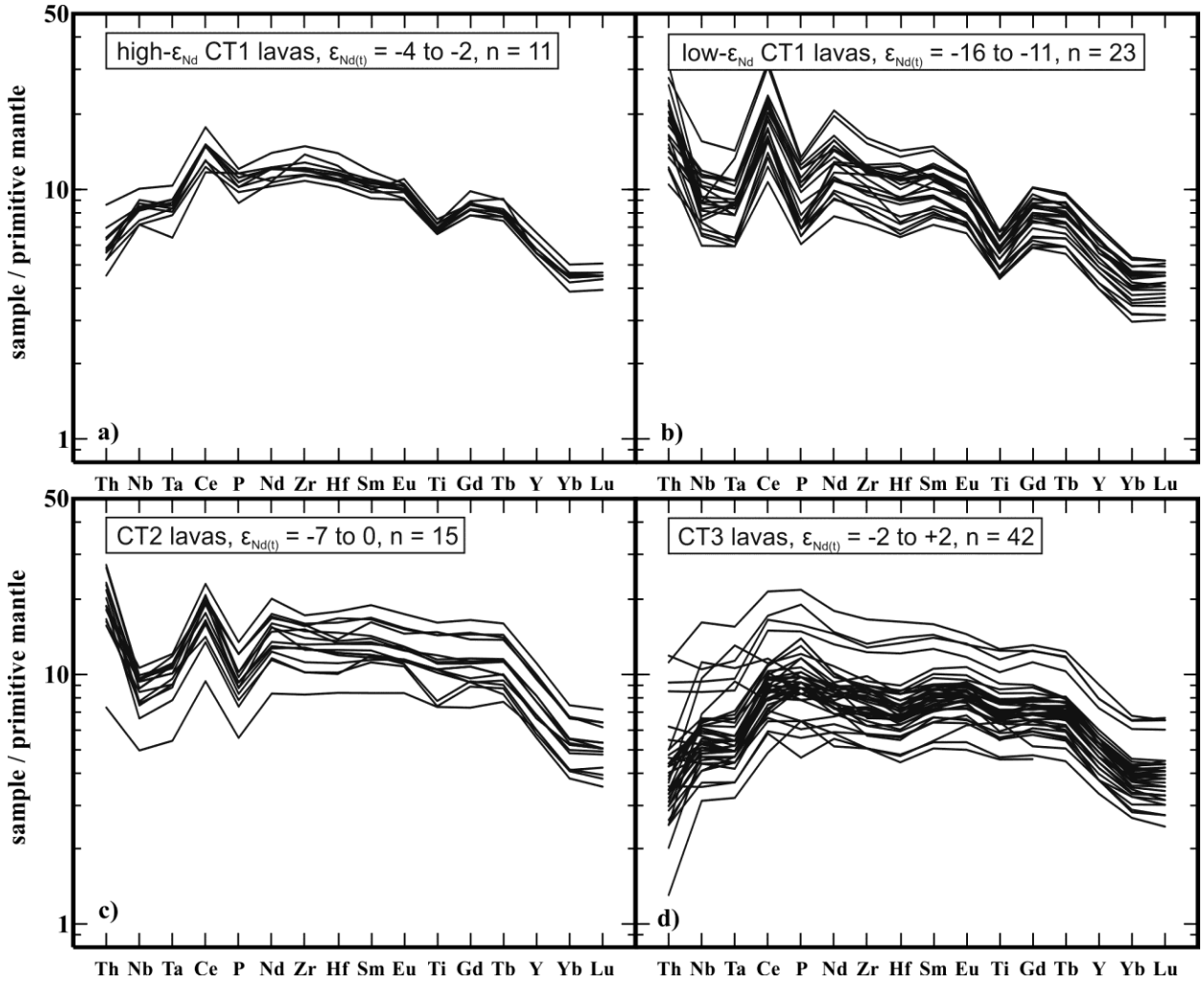

Fig. 4. Primitive-mantle-normalized (Sun and McDonough 1989) incompatible trace element patterns and Nd isotopic compositions shown for the different Vestfjella CT magma types (Luttinen and Siivola 1997; Luttinen et al. 1998; Luttinen and Furnes 2000).

Vestfjella CFBs

The Vestfjella mountain range is composed of a ~130 km long NE-SW trending discontinuous chain of nunataks close to the Weddell Sea shoreline at western Dronning Maud Land (Fig. 2a). The nunataks are almost exclusively composed of tholeiitic rift-assemblage Karoo CFBs that have a stratigraphic thickness in excess of 1 km (e.g., Furnes et al. 1987; Luttinen and Furnes 2000). On the basis of U-Pb and $^{40}Ar/^{39}Ar$ dating of the crosscutting dikes, the CFBs are older than 182 Ma, possibly >187 Ma, i.e. they may represent the earliest eruptions related to the emplacement of the Karoo province (Luttinen et al. 2015). The base of the CFB succession is not exposed at Vestfjella, but the lithospheric boundary between Maud Belt and Grunehogna craton has been interpreted to underlie the study area (Fig. 2; Corner 1994).

The Vestfjella CFBs show a wide range of trace element and Nd isotopic variation ($\varepsilon_{Nd(t)}$ from -16 to +2) that is nearly equal to that of the Karoo CFBs as a whole (Figs. 3b and 4). On the basis of Ti-Zr-P systematics and Nd isotopic composition, they can be divided into four *chemical types* (CT) that represent geochemically distinct magma types: high-ε_{Nd} CT1, low-ε_{Nd} CT1, CT2, and CT3 (Luttinen and Siivola 1997; Luttinen et al. 1998; Luttinen and Furnes 2000).

CT1 lavas dominate the northern parts of Vestfjella, show low Ti/Zr (< 80) and Ti/P (≤ 13): the ***high-ε_{Nd} CT1 lavas*** ($\varepsilon_{Nd(t)}$ from -4 to -2) exhibit low Th/Ta (1–2), whereas the ***low-ε_{Nd} CT1 lavas*** ($\varepsilon_{Nd(t)}$ from -16 to -11) exhibit high Th/Ta (3–7). ***CT2 lavas***, a volumetrically minor component mainly found in northern Vestfjella, show high Ti/Zr (80–120), Ti/P (13–20) and Th/Ta (3–5), and $\varepsilon_{Nd(t)}$ from -7 to 0. ***CT3 lavas*** dominate southern Vestfjella and exhibit high Ti/Zr (80–180), low Ti/P (7–14) and Th/Ta (1–3), and $\varepsilon_{Nd(t)}$ from -2 to +2. These and other geochemical differences between the different magma types are readily illustrated in Figs. 3b and 4.

The intrusive rocks of Vestfjella include gabbros (Vuori and Luttinen 2003), ferropicrite dikes (Heinonen and Luttinen 2008, 2010; Heinonen et al. 2010), and lamproite dikes (Luttinen et al. 2002). Most of the intrusive rocks, however, are tholeiitic dikes that exhibit large geochemical variations, from incompatible element-enriched CT1-type ($\varepsilon_{Nd(t)}$ = -18) to dikes relatively depleted in the most incompatible elements (the so-called "Low-Nb" magma type; $\varepsilon_{Nd(t)}$ from +7 to +8; Fig. 3) (Furnes et al. 1982; Luttinen et al. 1998, 2015; Luttinen and Furnes 2000). The MORB-like Low-Nb magma type is of fundamental importance as it has been interpreted to represent high-pressure melts from depleted sublithospheric mantle sources akin to those that produce the modern SWIR MORBs (Heinonen et al. 2010; Luttinen et al. 2015) and it seems to correspond to a depleted end-member composition of Karoo CFBs in Sr-Nd isotopic space (Fig. 3b).

Geochemical studies have ascribed the general major and trace element variability in the Vestfjella CFBs to fractional crystallization process and concluded that the origin of the distinctive magma types required either contamination, source heterogeneity, or both (Furnes et al. 1987; Luttinen et al. 1998; Luttinen and Furnes 2000). Luttinen and Furnes (2000) favored separate and variably enriched mantle sources for the lavas, largely based on the excessive degrees of crustal contamination (>20 wt. %) inferred from AFC models. Subsequent accumulation of isotopic data (Luttinen et al. 2010, 2015) has demonstrated that the geochemical trends of the Antarctic Karoo lavas and related dikes also tend to converge toward a DM-like composition, which may suggest a common source end-member.

Constraining the model parameters

Our EC-AFC and AFC modeling focused on a wide selection of incompatible trace elements (Th, Nb, Ta, Ce, P, Nd, Zr, Hf, Sm, Eu, Ti, Gd, Tb, Y, Yb, and Lu) and Nd isotopic compositions that are not easily modified by secondary alteration, the evidence of which has been observed in the Vestfjella CFBs (Furnes et al. 1987; Luttinen and Furnes 2000). They also suffice to define the characteristic features of the magma types. The compositions, thermodynamic properties, and bulk partition coefficients (D) for the parental magma and contaminants are discussed below and presented in Tables 1–2.

Constraining the parental melt compositions

We used the whole-rock geochemical data of the uncontaminated MORB-affinity Low-Nb dikes (Heinonen et al. 2010; Luttinen et al. 2015) to constrain the parental melt compositions. The dikes do not likely represent parental melts *sensu stricto*, however, as they mostly have basaltic MgO contents (7–12 wt. %; one olivine cumulate sample with MgO = 20 wt. %). Furthermore, they show higher $(Sm/Yb)_N$ (2.3–2.6) than the least enriched (but still lithosphere-signatured) Vestfjella lavas (1.9; Fig. 5). We ascribe the higher Sm/Yb of the crosscutting dikes to relatively lower degrees of partial mantle melting after the voluminous main flood basalt phase (see Luttinen et al. 2015).

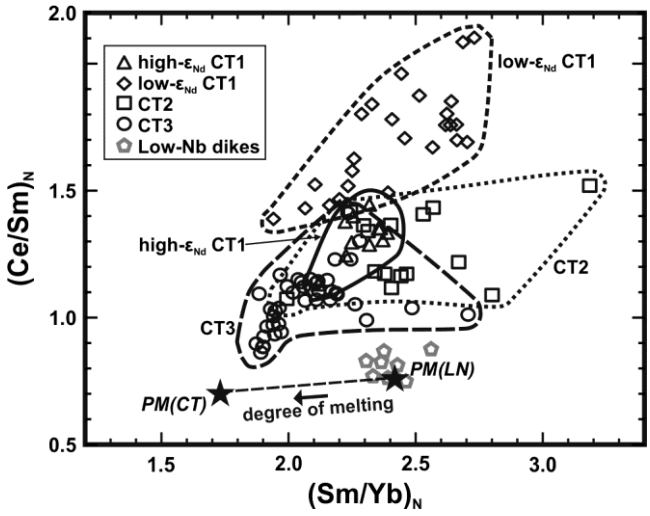

Fig. 5. Chondrite-normalized (McDonough and Sun 1995) Sm/Yb vs. Ce/Sm for the Low-Nb dikes, different Vestfjella CT magma types, and parental melts for the Low-Nb dikes (PM_{LN}) and CT lavas (PM_{CT}; reconstruction in Table 1 and Fig. 6).

First, a parental major and trace element melt composition was calculated for the Low-Nb dikes (PM_{LN}) by adding liquidus olivine to the most isotopically depleted Low-Nb dike sample (P27-AVL; $\varepsilon_{Nd(t)}$ = +7.7) until the calculated melt reached equilibrium with depleted mantle olivine (Fo_{90}; Workman and Hart 2005). Fractionation of olivine does not have a significant effect on incompatible trace element ratios and PM_{LN} has $(Sm/Yb)_N$ of 2.4 similar to those of Low-Nb dikes (Fig. 5). Degree of melting (especially in the presence of garnet), on the other

hand, has a significant effect on the concentrations of heavy REE in the melt. Because the Low-Nb dikes likely represent lower degrees of mantle melting than the lavas, as noted above, the trace element composition of the parental melt for the lavas (PM_{CT}) was calculated by assuming a degree of melting that was twice as high (F = 12 %) as that indicated by rare earth element (REE) modeling of the PM_{LN} (F = 6 %; assuming modal batch melting of an E-DMM source; Workman and Hart 2005; Table 1; Fig. 6). The reconstructed PM_{CT} has $(Sm/Yb)_N$ of 1.7, slightly lower than that of the least contaminated lavas, and thus we consider its trace element composition to represent a reasonable parental melt composition for the lavas (Fig. 5). We emphasize that the degrees of melting (6 and 12 %) are based on simple modal batch melting modeling and should thus not be considered as absolute values; they are only used to estimate the effect of variable partial melting on the geochemistry of the primary magmas. Thermodynamic parameters for the high-degree parental melt were constrained by using major element composition of a very Mg-rich CFB-related melt reported by Thompson and Gibson (2000).

Constraining the lithospheric contaminant compositions

Crustal contaminants were chosen to represent the Precambrian basement of southern Gondwana in cases where sufficient geochemical data were available. We performed simple AFC modeling (not presented here) to test the suitability of the different rock types as contaminants for the Vestfjella lavas. The compositions of the best-fit contaminants are listed in Table 2 and were chosen based on comparison between the preliminary model results and observed trace element characteristics.

The preliminary upper crust dataset included Archean tonalite–trondhjemite–granodiorite (TTG) gneisses and metasedimentary rocks from Africa (Kreissig et al. 2000), Proterozoic Ritscherflya metasedimentary rocks (Moyes et al. 1995; Perritt 2001) and Borgmassivet intrusions (Riley and Millar 2014) that overlie the Archean craton in western Dronning Maud Land, Proterozoic and Paleozoic gneisses related to the Maud Belt (Wareham et al. 1998; Will et al. 2010; Grantham et al. 2011), and a global average upper crust composition (Rudnick and Gao 2003).

Comprehensive geochemical data for lower crust of the area are not available, and thus our preliminary dataset included the granulites of the Ross Orogen of northern Victoria Land (Talarico et al. 1995; Antonini et al. 1999), granulites from the North China Craton that is characterized by an Archean core and is lithologically similar to the basement of the study area (Yu et al. 2003; Ying et al. 2010; Jiang et al. 2011), and a global average lower crust composition (Rudnick and Gao 2003).

Local ~160 Ma lamproites from Vestfjella (Luttinen et al. 2002), carbonatites, nephelinites, and ijolites related to Kaapvaal SCLM and its surroundings (Harmer et al. 1998; Harmer 1999), and average lamproite (Bergman 1987) were selected to represent partial melt compositions of the local fertile SCLM for AFC modeling.

Heinonen, J.S., Luttinen, A.V., Bohrson, W.A. 2016. Enriched continental flood basalts from depleted mantle melts: modeling the lithospheric contamination of Karoo lavas from Antarctica. Contributions to Mineralogy and Petrology 171:9. http://dx.doi.org/10.1007/s00410-015-1214-8 (Author's postprint)

Table 1 Details of the parental melt modeling

a) Major and trace element composition for the parental melt of the MORB-like low-Nb dikes

Majors: addition (33 wt. % in total) of equilibrium olivine ($K_d(Fe\text{-}Mg)^{ol\text{-}liq}$ = 0.35; Fe^{3+}/Fe_T = 0.1) to sample P27-AVL (Luttinen and Furnes 2000) in 1 wt.% steps until in equilibrium with MORB source olivine (Fo_{90}; Workman and Hart 2005):

	SiO_2	TiO_2	Al_2O_3	FeO_{tot}	MnO	MgO	CaO	Na_2O	K_2O	P_2O_5	
PM_{LN}	47.85	1.33	10.56	11.22	0.19	17.63	9.31	1.62	0.17	0.11	[wt. %]

Traces: addition of 33 wt.% of olivine to MORB-like dike sample P27-AVL (Luttinen and Furnes 2000) using K_d compilation after Boudreau (1999):

	Th	Nb	Ta	La	Ce	P	Nd	Zr	Hf	Sm	Eu	Ti	Gd	Tb	Y	Yb	Lu	
K_d	0.0003	0.0010	0.0010	0.0003	0.0003	0.0003	0.0002	0.0010	0.0029	0.0002	0.0002	0.0020	0.0003	0.0005	0.0010	0.0052	0.0085	
PM_{LN}	0.172	2.35	0.127	3.73	9.17	491	7.90	64.5	1.85	2.89	1.07	7970	3.26	0.593	16.5	1.30	0.195	[ppm]

b) Approximating the degree of partial modal batch melting of the parental melt of Low-Nb dikes on the basis of REE composition (Fig. 6):

E-DMM[#] source of Workman and Hart (2005):

	La	Ce	Pr	Nd	Sm	Eu	Gd	Tb	Dy	Ho	Er	Tm	Yb	Lu	
E-DMM	0.253	0.726		0.703	0.273			0.076					0.382	0.060	[ppm]

Bulk partition coefficients for the mantle source (57% olivine, 28% opx, 12% cpx, and 3% garnet) calculated following the compilation of Adam and Green (2006):

	La	Ce	Pr	Nd	Sm	Eu	Gd	Tb	Dy	Ho	Er	Tm	Yb	Lu
D_1	0.0049	0.0090		0.0214	0.0412			0.0924					0.2310	0.2543

Best fit to Low-Nb parental melt attained when degree of modal batch melting of the E-DMM source using D_1 values is **6%** (see Fig. 6):

	La	Ce	Pr	Nd	Sm	Eu	Gd	Tb	Dy	Ho	Er	Tm	Yb	Lu	
PM_{LN}	3.73	9.17		7.90	2.89	1.07	3.26	0.593					1.30	0.195	[ppm]
Model	3.92	10.61		8.77	2.77			0.518					1.38	0.201	[ppm]

Inferred bulk partition coefficients for the mantle source of PM_{LN} composed of E-DMM peridotite (Workman and Hart 2005) at F=6%:

	Th	Nb	Ta	La	Ce	P	Nd	Zr	Hf	Sm	Eu	Ti	Gd	Tb	Y	Yb	Lu	
E-DMM	0.016	0.246	0.016	0.253	0.726	-	0.703	6.09	0.186	0.273	0.108	792	0.397	0.076	3.55	0.382	0.060	[ppm]
D_2	0.0330	0.0477	0.0688	0.0084	0.0204	-	0.0309	0.0365	0.0433	0.0367	0.0433	0.0419	0.0659	0.0726	0.1649	0.2489	0.2627	

c) Major and trace element composition for the CT parental melt (twice the degree of melting (12%) compared to Low-Nb parental melt):

Majors: representative CFB-related high-Mg magma (Thompson and Gibson 2000; only used to provide rough estimates for the thermal parameters):

	SiO_2	TiO_2	Al_2O_3	FeO_{tot}	MnO	MgO	CaO	Na_2O	K_2O	P_2O_5	
PM_{CT}	46.30	0.70	9.00	12.00	0.20	24.00	6.50	1.10	0.10	0.10	[wt. %]

Traces: composition of the E-DMM modal batch partial melt at F=12% using D_2 values:

	Th	Nb	Ta	La	Ce	P*	Nd	Zr	Hf	Sm	Eu	Ti	Gd	Tb	Y	Yb	Lu	
PM_{CT}	0.105	1.52	0.088	1.99	5.26	290	4.78	40.0	1.18	1.79	0.683	5049	2.23	0.413	13.4	1.13	0.171	[ppm]

[#] E-DMM was chosen instead of average DMM, because some incompatible trace elements (e.g., Th and Ce) are slightly enriched in Low-Nb dikes relative to N-MORB (Fig. 3). * P assumed to be depleted in PM_{CT} as in PM_{LN} relative to Ce and Nd

Heinonen, J.S., Luttinen, A.V., Bohrson, W.A. 2016. Enriched continental flood basalts from depleted mantle melts: modeling the lithospheric contamination of Karoo lavas from Antarctica. Contributions to Mineralogy and Petrology 171:9. http://dx.doi.org/10.1007/s00410-015-1214-8 (Author's postprint)

Table 2 Details of the thermodynamical constraints, contaminant compositions, and bulk partition coefficients

Variable	**PM_{CT}[1]**	**Lower crust[2]**	**Archean TTG[3]**	**SCLM-1[4]**	**SCLM-2[5]**
Model	-	EC-AFC	EC-AFC	AFC (r=0.07)	AFC (r=0.2)
Magma liquidus T (initial T) [°C]	1500	-	-	-	-
Assimilant liquidus T [°C]	-	1100	1000	-	-
Assimilant initial T [°C]	-	800	700	-	-
Solidus T [°C]	-	950	850	-	-
Equilibration T [°C]	-	1080	980	-	-
Isobaric specific heat [J/kg K]	1650	1388	1370	-	-
Crystallization enthalpy [J/Kg]	450000	-	-	-	-
Fusion enthalpy [J/Kg]	-	350000	270000	-	-
Th [ppm]	0.105	0.11	3.6	46	0.80
D (Th)	0.0003	0.1/0.5	0.1/0.5	-	-
Nb [ppm]	1.52	11.7	5	95	8.5
D (Nb)	0.001	0.1/0.5	0.1/0.5	-	-
Ta [ppm]	0.088	0.43	0.3	4.7	0.5
D (Ta)	0.001	0.1/0.5	0.1/0.5	-	-
Ce [ppm]	5.26	88.73	64	400	45.35
D (Ce)	0.0003	0.1/0.5	0.1/0.5	-	-
P [ppm]	290	2255	698	3098	4535
D (P)	0.0003	0.1/0.5	0.1/0.5	-	-
Nd [ppm]	4.78	47.73	22	207	22.97
D (Nd)	0.0002	0.1/0.5	0.1/0.5	-	-
Zr [ppm]	40	357	132	922	72
D (Zr)	0.001	0.1/0.5	0.1/0.5	-	-
Hf [ppm]	1.18	8.31	3.04	39	1.57
D (Hf)	0.0029	0.1/0.5	0.1/0.5	-	-
Sm [ppm]	1.79	9.53	3.52	24	4.09
D (Sm)	0.0002	0.1/0.5	0.1/0.5	-	-
Eu [ppm]	0.683	2.66	1.01	4.8	1.32
D (Eu)	0.0002	0.1/0.5	0.1/0.5	-	-
Ti [ppm]	5049	8153	1737	17985	6295
D (Ti)	0.002	0.1/0.5	0.1/0.5	-	-
Gd [ppm]	2.23	7.39	3.8	13	4.11
D (Gd)	0.0003	0.1/0.5	0.1/0.5	-	-
Tb [ppm]	0.413	1.02	0.4	1.4	0.56
D (Tb)	0.0005	0.1/0.5	0.1/0.5	-	-
Y [ppm]	13.4	23.7	10	27	15
D (Y)	0.001	0.1/0.5	0.1/0.5	-	-
Yb [ppm]	1.13	2.44	0.5	1.7	0.26
D (Yb)	0.0052	0.1/0.5	0.1/0.5	-	-
Lu [ppm]	0.171	0.36	0.1	0.23	0.04
D (Lu)	0.0085	0.1/0.5	0.1/0.5	-	-
$(^{143}Nd/^{144}Nd)_{180\ Ma}^{MAX}$	0.512829	-	0.5109	0.512129*	0.512129*
$(^{143}Nd/^{144}Nd)_{180\ Ma}^{MIN}$	0.512829	-	0.51026	0.511326#	0.511326#

(1) Sources for the parental melt (PM_{CT}) parameters: For the estimation of magma liquidus T, see text; Isobaric specific heat calculated on the basis of major element composition presented in Table 1 using the partial molar isobaric heat capacities listed by Spera and Bohrson (2001); Crystallization enthalpy estimated using equilibrium crystallization model for the major element composition presented in Table 1 at 2 kbar (with Cr_2O_3 = 0.3 wt. %) in PELE software (Boudreau 1999). The D values for the fractionation of olivine from the parental magmas are based on those used in the PELE modeling software of Boudreau (1999).

(2) Sources for the lower crust composition: Thermodynamical parameters represent the standard lower crustal values of Bohrson and Spera (2001), except for the initial temperatures that represent values compatible with active continental rift environment (see Bohrson and Spera 2001; Chapman 1986); Trace element composition after average of granulite samples 05LG10, 05LG16, and 05LG17 from the North China craton (Ying et al. 2010); Nd isotopic data not available.

(3) Sources for the Archean TTG composition: Thermodynamical parameters represent the standard upper crustal values of Bohrson and Spera (2001), except for the initial temperatures that represent values compatible with active continental rift environment (see Bohrson and Spera 2001; Chapman 1986); Trace element composition after TTG sample 96/203 from the Kaapvaal craton (Kreissig et al. 2000; Ta and Hf estimated relative to Nb and Zr, respectively, using ratios of Lana et al. 2004); Nd isotopic composition after the range reported for the TTGs of the area (Kreissig et al. 2000).

(4) Sources for the SCLM-1 partial melt composition: Trace element composition after average lamproite of Bergman (1987); Nd isotopic composition after the range reported for the alkaline rocks described in Harmer et al. (1998) and Luttinen et al. (2002); * back-calculated at 159 Ma (Luttinen et al. 2002); # back-calculated at 190 Ma (Harmer et al. 1998)

(5) Sources for the SCLM-2 partial melt composition: Trace element composition after a representative Spitskop ijolite (S115; Harmer 1999) with Ta and Hf estimated using Nb/Ta = 17 and Zr/Hf = 46 (Chakhmouradian 2006), Th estimated using Nb/Th = 10.64 (after Buhera ijolites; Harmer et al. 1998), and Tb estimated relative to other REE; Nd isotopic composition after the range reported for the alkaline rocks described in Harmer et al. (1998) and Luttinen et al. (2002);

* back-calculated at 159 Ma (Luttinen et al. 2002); # back-calculated at 190 Ma (Harmer et al. 1998)

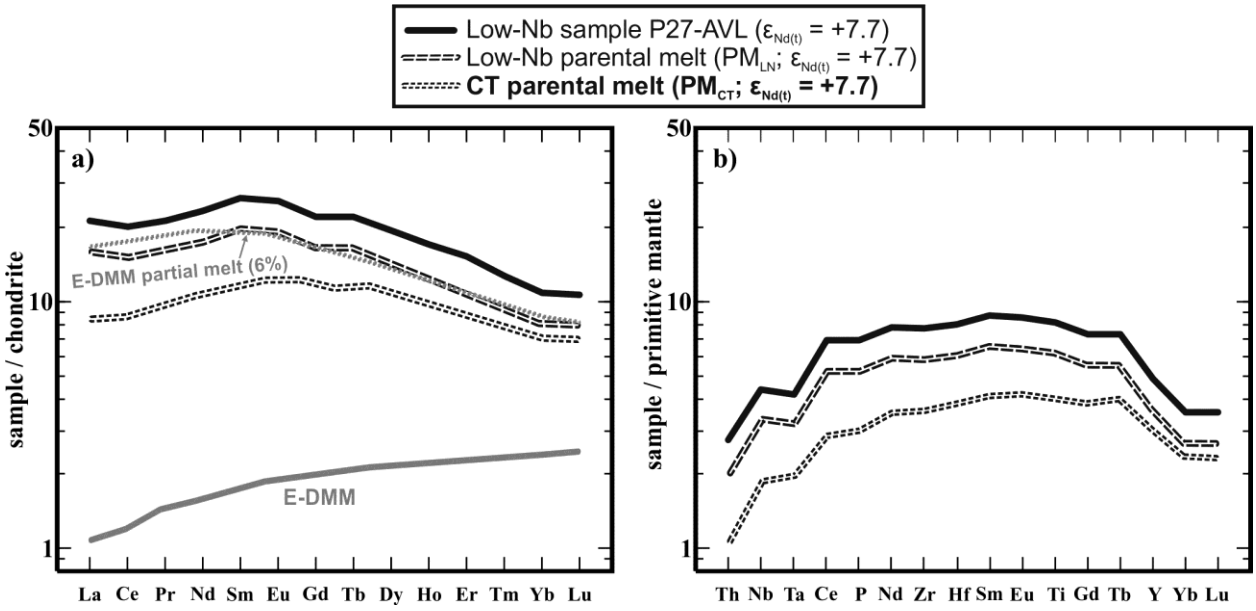

Fig. 6. (a) Reconstruction of the parental melt composition for the CT lavas presented in chondrite-normalized (McDonough and Sun 1995) REE diagram: Parental melt for the Vestfjella lavas (PM_{CT}) has been calculated by assuming 12% of melting of E-DMM source (Workman and Hart 2005) using D values that were constrained so that the parental melt of Low-Nb dikes (PM_{LN}; calculated by adding 33 wt.% of equilibrium olivine to sample P27-AVL) represents a 6% partial melt of the E-DMM source, as indicated

by the best-fit melting model (Table 1). (b) Primitive-mantle normalized (Sun and McDonough 1989) incompatible trace element patterns of the Low-Nb dike sample P27-AVL, PM_{LN}, and PM_{CT} (Table 1).

Constraining the thermodynamic parameters

Conventional thermometers based on olivine-liquid equilibrium yield extremely high liquidus temperatures of >1600 °C for the most magnesian magmas of the Karoo province (Heinonen and Luttinen 2010). The recently developed of Al-in-olivine thermometer is independent of pressure and melt composition, and indicates that the conventional thermometers may overestimate the actual temperatures by ~100 °C (Heinonen et al. 2015). Accordingly, we have used a liquidus T of 1500 °C for the parental melt in the model (Table 2). The isobaric specific heat was constrained using the partial molar isobaric heat capacities listed by Spera and Bohrson (2001) and the crystallization enthalpy was constrained by equilibrium crystallization modeling in PELE software (Boudreau 1999) using the approximated parental magma major element composition (Table 2).

The thermodynamic properties of the crustal contaminants represent the standard upper and lower crustal cases of Bohrson and Spera (2001), except for the initial temperatures that take into account the heating effect of mafic underplating in a continental rift environment (Chapman 1986; Table 2). Equilibration temperature (i.e. the natural variable describing the approach to equilibrium during heat exchange; Spera and Bohrson 2001) was chosen to be 20°C below the wallrock liquidus (Table 2; Bohrson and Spera 2001). These temperatures (1080 °C for the lower crustal contaminant and 980 °C for the upper crustal contaminant) are slightly lower than the estimated eruption temperature of ~1100 °C that we calculated for the most evolved Vestfjella CFB magma composition (CT2 sample B408-AVL; Luttinen and Furnes 2000) on the basis of MELTS algorithms (Ghiorso and Sack 1995). The lack of more evolved compositions in the Vestfjella lava succession indicates that the heat exchange in the system was limited to the close vicinity of the fractionating magma chambers (see Spera and Bohrson 2001).

Due to lack of data regarding the thermodynamic properties of the lithospheric mantle, subcontinental mantle contamination was modeled as an AFC process using the equations of DePaolo (1981b), which do not conserve energy or mass. We approximated the partial melting of such wallrock by using rock compositions that represent the partial melts of local metasomatized SCLM as contaminants (see previous section).

Constraining the partition coefficients

The D values for the fractionation of olivine from the parental magmas are based on those used in the PELE modeling software of Boudreau (1999) and are listed in Table 2. The D values for the crustal contaminants (D_c) are difficult to estimate in detail given the possible variation in source mineralogy and the dependence of element partitioning on melting conditions. All the modeled elements are likely to behave incompatibly during crustal anatexis in general, however (e.g., Bea 1996; Nash and Crecraft 1985), and thus we used constant D_c values of 0.1 and 0.5 for all the elements in two separate model runs (Table 2). We consider that the feasible D_c values for the modeled elements are likely to be bracketed within this range. Using constant D_c values leads to underestimation of inter-element fractionation during wall-rock melting, but we favored such an approach over aforementioned uncertainties.

Modeling of the contamination of the Vestfjella CFBs

We emphasize that the intent of the models is to examine limits for mass balance between an asthenosphere-derived parental melt and the variety of lithospheric sources exposed in or estimated for the area, and thus the effect of, e.g., magma recharge is not used in the modeling. We only considered the most promising contaminants (chosen on the basis of geochemical comparison and preliminary AFC modeling, see previous section; Table 2).

The EC-AFC and AFC models do not directly track major element and phase equilibria evolution, but the amount of precipitated cumulates in the models (~10–40 wt. %; Table 3) indicates picritic to basaltic magma compositions. Mild variations in the degree of melting of the mantle source (and the contaminant) and fractional crystallization of olivine (± pyroxene and plagioclase) from the melt have significant influence on the absolute concentrations of trace elements included in the models, but have a small effect on their relative abundances. Therefore, it is the shapes of the observed vs. modeled trace element patterns that are more important than the absolute values in comparing them to the measured CFB compositions.

We have rated the results by comparing the modeled compositions to the average compositions of each CT magma type. The differences were quantified using a double-normalization procedure (Table 3; Figs. 7–10): First, we calculated primitive mantle-normalized trace element values for each of the modeled element compositions (insets a and b in Figs. 7–9, inset a in Fig. 10). Second, these values were normalized to the primitive mantle-normalized compositions of the average CT magma types assuming a double-normalized value of 1 for moderately incompatible Sm (insets c and d in Figs. 7–9, inset b in Fig. 10). Finally, the best-fit model results were identified on the basis of the lowest sum of residuals (Table 3). Such a procedure enables us to identify the results that provide the best match to the characteristic shapes of the trace element patterns of the magma types rather than the trace element concentrations. Three best-fit model results are highlighted for EC-AFC models with $D_c(x) = 0.1$ and for AFC models with $r = 0.07$, and five best-fit model results are highlighted for EC-AFC models with $D_c(x) = 0.5$ and for AFC model with $r = 0.2$. The $(Sm/Yb)_N$ vs. $(Ce/Sm)_N$ diagram (Fig. 11) is utilized to illustrate the effects of degree of melting in the source and Nd vs. $\varepsilon_{Nd(t)}$ diagram (Fig. 12) is utilized to illustrate the isotopic variation of the models.

Contamination of high-ε_{Nd} CT1 basalts by Proterozoic Lower Crust

The high-ε_{Nd} CT1 lavas exhibit a combination of relatively low Nb, Ta, P, and Ti contents (Fig. 4a) that can be attributed to interaction with crustal materials. Furthermore, relatively low Th is suggestive of the contaminant being lower rather than upper continental crust (e.g., Rudnick and Gao 2003). Our EC-AFC modeling suggests that 1–8 wt. % contamination (percent is relative to initial mass of magma body) of the parental magma with a lower crustal granulite (xenoliths from the North China Craton (Ying et al., 2010) gave the best-fit results) yields trace element patterns that are quite similar to that of the high-ε_{Nd} CT1, especially among elements from Ce to Lu (Figs. 7 and 11). The relatively high deviation at Th and Ta imply that the lower crustal contaminant of the high-ε_{Nd} CT1 basalts was more enriched in these elements than the composition used in the model, however.

The degrees of contamination suggested by the trace element modeling infer that the contaminant should have $\varepsilon_{Nd(t)}$ from -13 to -7 to match the $\varepsilon_{Nd(t)}$ values of the high-ε_{Nd} CT1 lavas

(from -4 to -2; Fig. 12a). Such Nd isotopic compositions correspond to T_{DM} model ages of 1.39–2.07 Ga, which were calculated using average Sm/Nd of the xenoliths (0.1997) and DM evolution models of DePaolo (1981a) and Goldstein et al. (1984). The model ages suggest that the potential contaminant was Proterozoic rather than Archean in age.

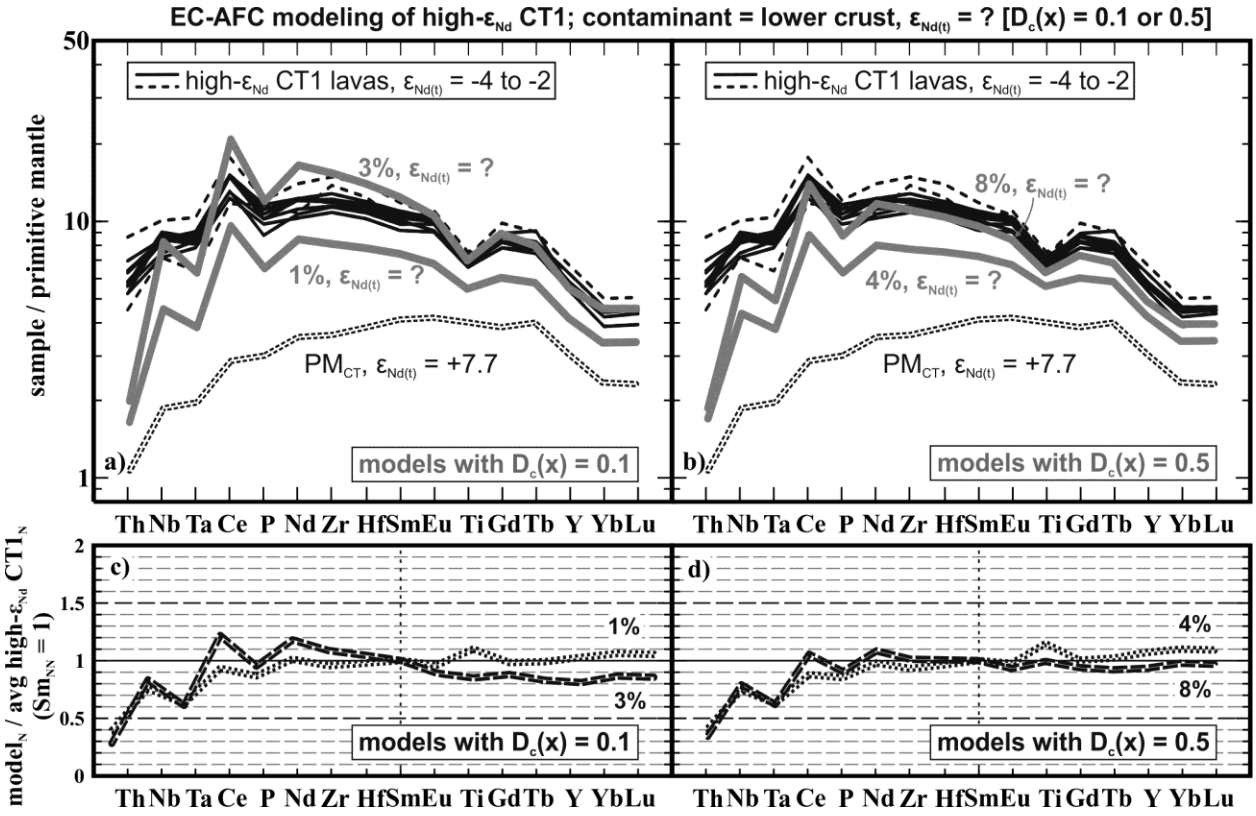

Fig. 7. Best-fit EC-AFC contamination (lower crust) model results for the high-ε_{Nd} CT1 lavas (see Tables 2 and 3). Percentages indicate the mass of the assimilated material relative to mass of the original melt (M_a). a) Primitive-mantle-normalized (Sun and McDonough 1989) contamination models with $D_c(x) = 0.1$; 2% model not shown to preserve clarity, but it would plot between the 1% and 3% patterns. Parental melt (PM_{CT}) and high-ε_{Nd} CT1 lavas (anomalous compositions indicated with stippled lines) also shown. b) Primitive-mantle-normalized (Sun and McDonough 1989) contamination models with $D_c(x) = 0.5$; 5–7% models not shown to preserve clarity, but they would plot between the 4% and 8% patterns. Parental melt (PM_{CT}) and high-ε_{Nd} CT1 lavas (anomalous compositions indicated with stippled lines) also shown. c) Double-normalized trace element patterns of the 1% and 3% models ($D_c(x) = 0.1$); the model compositions were first normalized to primitive mantle, and then to primitive-mantle-normalized average magma type composition (calculated on the basis of representative samples) so that model $Sm_{NN} = 1$. d) Double-normalized trace element patterns of the 4% and 8% models ($D_c(x) = 0.5$).

Contamination of low-ε_{Nd} CT1 basalts by Archean TTGs

The combination of relatively high Th and low Nb, Ta, P, and Ti of the low-ε_{Nd} CT1 lavas (Fig. 4b) is compatible with interaction of the parental magmas with upper continental crust (see, e.g., Rudnick and Gao 2003). The notably low initial $\varepsilon_{Nd(t)}$ of the basalts (-16 to -11) indicates that the crustal component was of Archean age. EC-AFC models with 2–15 wt. % ($D_c(x) = 0.1–0.5$)

contributions from Archean TTG gneiss from the associated Kaapvaal craton (Kreissig et al. 2000) result in trace element patterns that are notably similar to that of the basalts (Fig. 8; Table 3). Using the range of Kaapvaal TTG Nd isotopic compositions reported by Kreissig et al. (2000) in the model yields a range of $\varepsilon_{Nd(t)}$ values (-23 to -10) that encompasses those measured from the basalts (Figs. 8 and 12b).

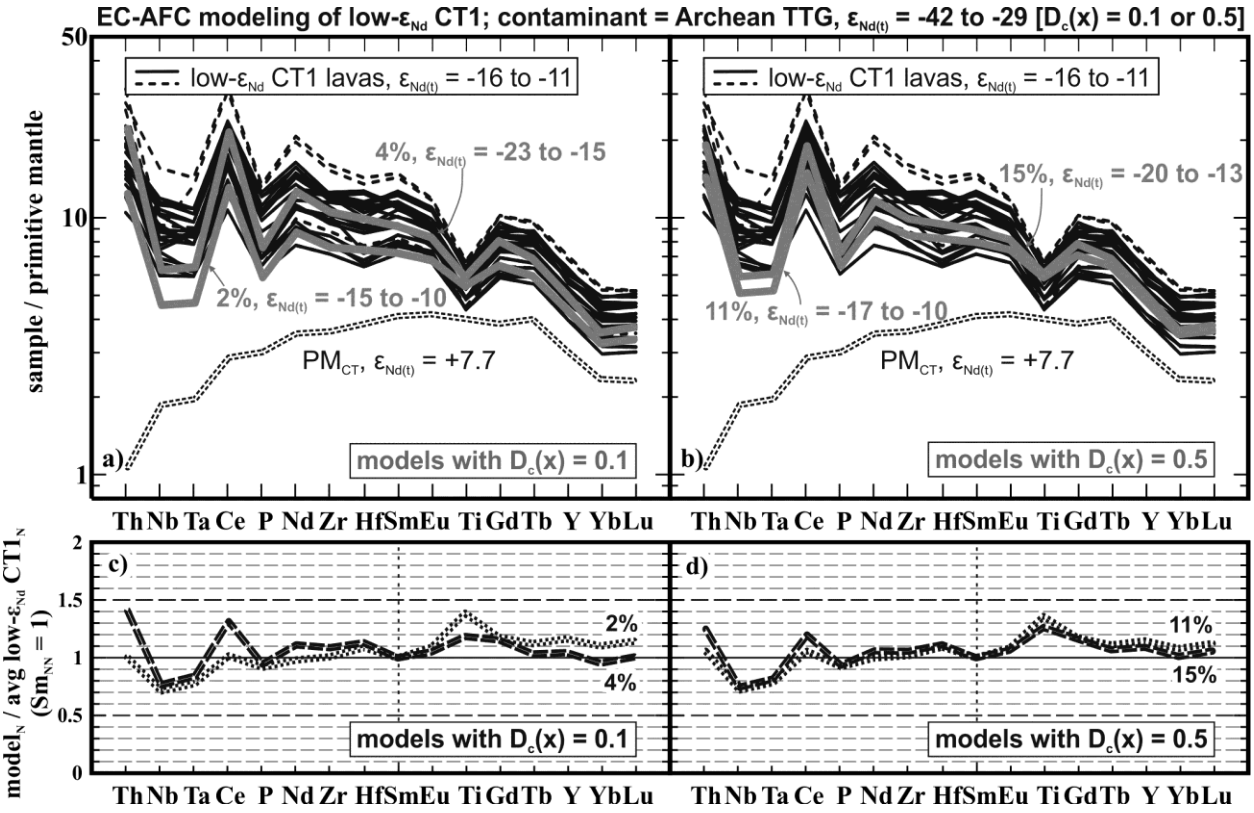

Fig. 8. Best-fit EC-AFC contamination (Archean TTG) model results for the low-ε_{Nd} CT1 lavas (see Tables 2 and 3). Percentages indicate the mass of the assimilated material relative to mass of the original melt (M_a). a) Primitive-mantle-normalized (Sun and McDonough 1989) contamination models with $D_c(x) = 0.1$; 3% model not shown to preserve clarity, but it would plot between the 2% and 4% patterns. Parental melt (PM_{CT}) and low-ε_{Nd} CT1 lavas (anomalous compositions indicated with stippled lines) also shown. b) Primitive-mantle-normalized (Sun and McDonough 1989) contamination models with $D_c(x) = 0.5$; 12–14% models not shown to preserve clarity, but they would plot between the 11% and 15% patterns. Parental melt (PM_{CT}) and low-ε_{Nd} CT1 lavas (anomalous compositions indicated with stippled lines) also shown. c) Double-normalized trace element patterns of the 2% and 4% models ($D_c(x) = 0.1$); the model compositions were first normalized to primitive mantle, and then to primitive-mantle-normalized average magma type composition (calculated on the basis of representative samples) so that model $Sm_{NN} = 1$. d) Double-normalized trace element patterns of the 11% and 15% models ($D_c(x) = 0.5$).

Contamination of CT2 basalts by metasomatized SCLM

The trace element characteristics of the CT2 lavas (relatively low Nb, Ta, and P, but no negative Ti anomaly; Fig. 4c) indicate interaction with either a crustal contaminant having relatively high Ti or SCLM.

Our models indicate that incorporation of 1–3 wt. % of lamproite (average of Bergman 1987) produces daughter magmas that exhibit trace element patterns and isotopic compositions that are quite similar to those of the CT2 lavas, although the modeled Sm/Yb are lower and Th contents higher (at high degrees of contamination) than in CT2 (Figs. 9a, c, 11c, and 12c; Table 3). The difference in Sm/Yb suggests that parental magma or the contaminant was more depleted in heavy REE. For example, using the parental melt of the Low-Nb dikes (PM_{LN}; Table 1) as the starting composition the models yield better match for CT2 lavas having higher Sm/Yb (Fig. 11c) and also a better fit in terms of trace element ratios and their concentrations (Figs. 9b, d, and 11c; Table 3). It is possible that the wide range of Sm/Yb in the CT2 lavas results from variable degrees of melting and that their parental melts extended to higher Sm/Yb (i.e. lower degree of melting) than the one used in the other models (PM_{CT}; Fig. 11). In fact, CT2 represents a volumetrically minor magma type and the lavas may well have originated from isolated and compositionally distinct melt batches that are not related to each other by fractional crystallization (see Luttinen and Furnes 2000).

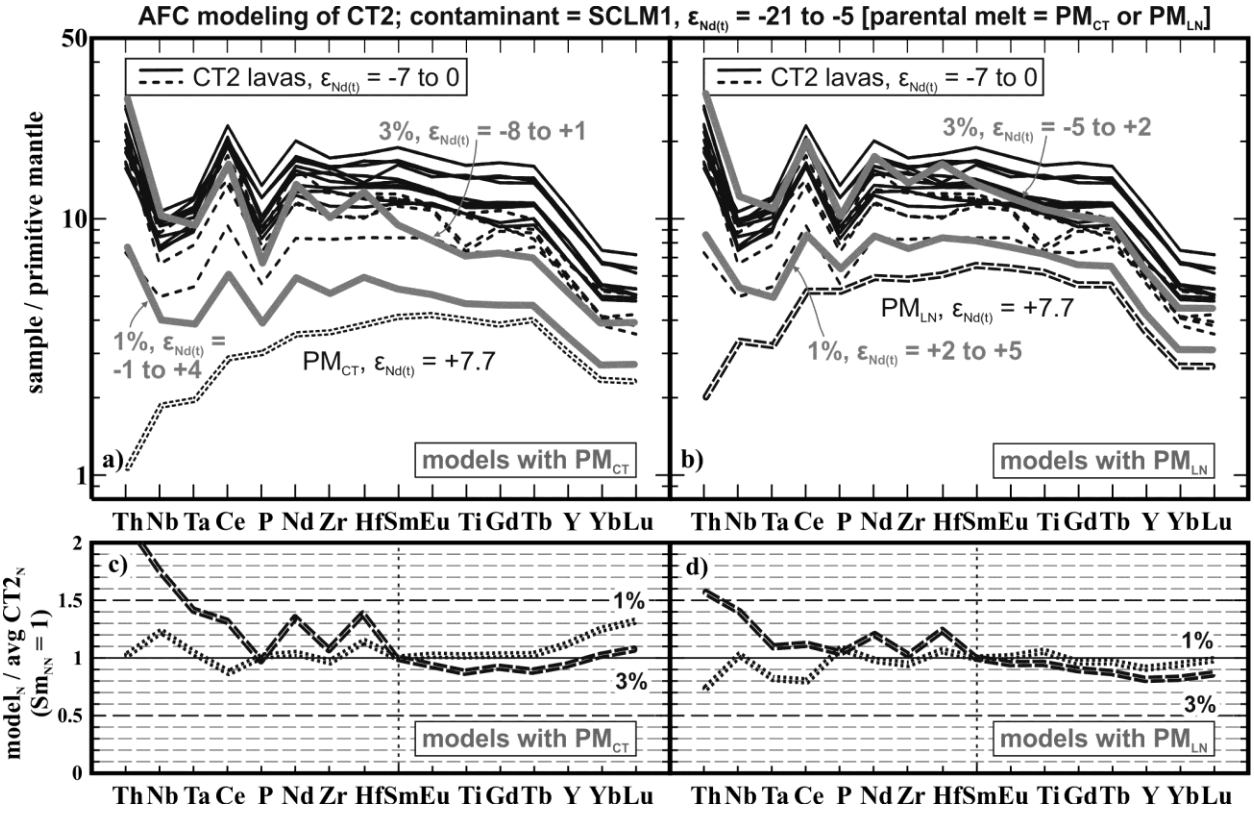

Fig. 9. Best-fit AFC contamination (SCLM1) model results for the CT2 lavas (see Tables 2 and 3). Percentages indicate the mass of the assimilated material relative to mass of the original melt (M_a). a) Primitive-mantle-normalized (Sun and McDonough 1989) contamination models with PM_{CT}; 2% model not

shown to preserve clarity, but it would plot between the 1% and 3% patterns. Parental melt (PM_{CT}) and CT2 lavas (anomalous compositions indicated with stippled lines) also shown. b) Primitive-mantle-normalized (Sun and McDonough 1989) contamination models with PM_{LN}; 2% model not shown to preserve clarity, but it would plot between the 1% and 3% patterns. Parental melt (PM_{LN}) and low-ε_{Nd} CT1 lavas (anomalous compositions indicated with stippled lines) also shown. c) Double-normalized trace element patterns of the 1% and 3% models (PM_{CT}); the model compositions were first normalized to primitive mantle, and then to primitive-mantle-normalized average magma type composition (calculated on the basis of representative samples) so that model Sm_{NN} = 1. d) Double-normalized trace element patterns of the 1% and 3% models (PM_{LN}).

Contamination of CT3 basalts by metasomatized SCLM

The CT3 basalts are notably different from the other Vestfjella basalts by showing a much smoother trace element pattern with a diagnostic enrichment in P and relatively high $\varepsilon_{Nd(t)}$ (-2 to +2) (Fig. 4d). The incompatible trace element characteristics preclude significant interaction with crust and instead could indicate contamination by SCLM components. Specifically, the high P contents can be associated with portions of metasomatized lower SCLM (see Harmer et al. 1998; Harmer, 1999).

Our best-fit models involve an ijolitic contaminant from the metasomatized Kaapvaal SCLM (Harmer 1999). The notably close match between the observed and modeled trace element patterns indicates that 6–10 wt. % contamination with such material provides a feasible explanation for the characteristic features of CT3 (Fig. 10; Table 3). Using the range of Nd isotopic compositions reported for the metasomatized SCLM of the area (Harmer et al. 1998; Luttinen et al. 2002) the modeling produces $\varepsilon_{Nd(t)}$ values from -1 to +5 which overlap those of CT3 and lend further support to this contamination scenario (Figs. 10 and 12d). Some anomalous CT3 samples have relatively high Sm/Yb, however, and their incompatible trace element concentrations are also clearly higher than in the models (Figs. 10, 11d and 12d). We propose that, as in the case of CT2, some of the parental melts of CT3 may have shown higher Sm/Yb due to lower degrees of melting (Fig. 11c). Alternatively, the contaminant could also have been more enriched in light REE than the ijolites used in our models because of lower degree of melting of the SCLM.

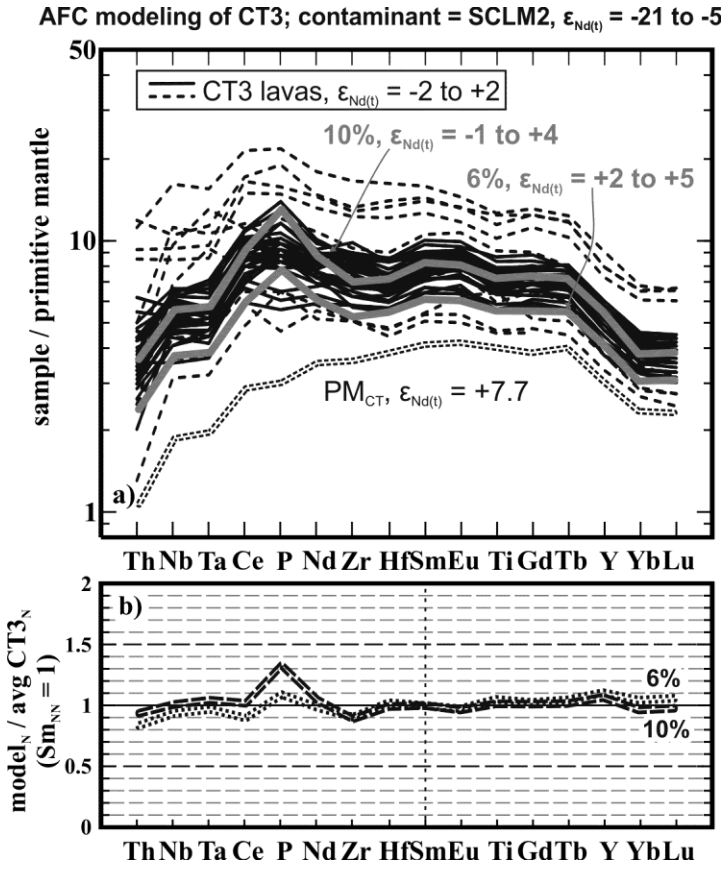

Fig. 10. Best-fit AFC contamination (SCLM2) model results for the CT3 lavas (see Tables 2 and 3). Percentages indicate the mass of the assimilated material relative to mass of the original melt (M_a). a) Primitive-mantle-normalized (Sun and McDonough 1989) contamination models; 7–9% models not shown to preserve clarity, but they would plot between the 6% and 10% patterns. Parental melt (PM_{CT}) and CT3 lavas (anomalous compositions indicated with stippled lines) also shown. b) Double-normalized trace element patterns of the 6% and 10% models; the model compositions were first normalized to primitive mantle, and then to primitive-mantle-normalized average magma type composition (calculated on the basis of representative samples) so that model Sm_{NN} = 1.

Table 3 Selected results of the contamination modeling (see Figs. 7–10 for illustration).

Magma type	model	contaminant	PM	$D_c(x)$	M_a	M_c	$error_{avg}$ (Sm_{NN} = 1)	$residuals^2$ (Sm_{NN} = 1)	$\varepsilon_{Nd(i)}$
high-ε_{Nd} CT1	EC-AFC	Lower crust	PM_{CT}	0.1	**1 %**	**18 %**	**11.32 %**	**0.61**	**?**
$\varepsilon_{Nd(i)}$ =					**2 %**	**21 %**	**13.62 %**	**0.72**	**?**
-4 to -2					**3 %**	**23 %**	**17.92 %**	**0.94**	**?**
					4 %	*25 %*	*20.93 %*	*1.15*	*?*
					5 %	*27 %*	*22.96 %*	*1.33*	*?*
					6 %	*29 %*	*24.32 %*	*1.46*	*?*
					7 %	*30 %*	*25.56 %*	*1.58*	*?*
					8 %	*31 %*	*26.36 %*	*1.66*	*?*

					9 %	*33 %*	*27.28 %*	*1.75*	*?*
					10 %	*34 %*	*27.88 %*	*1.82*	*?*
	EC-AFC	Lower crust	PM_{CT}	0.5	*1 %*	*18 %*	*22.25 %*	*1.07*	*?*
					2 %	*21 %*	*18.64 %*	*0.85*	*?*
					3 %	*23 %*	*15.60 %*	*0.71*	*?*
					4 %	**25 %**	**12.93 %**	**0.64**	**?**
					5 %	**27 %**	**11.24 %**	**0.61**	**?**
					6 %	**29 %**	**10.48 %**	**0.62**	**?**
					7 %	**30 %**	**10.52 %**	**0.63**	**?**
					8 %	**31 %**	**11.47 %**	**0.66**	**?**
					9 %	*33 %*	*13.00 %*	*0.70*	*?*
					10 %	*34 %*	*14.00 %*	*0.74*	*?*
low-ε_{Nd} CT1	EC-AFC	Archean TTG	PM_{CT}	0.1	*1 %*	*29 %*	*20.82 %*	*0.41*	*-7 to -3*
$\varepsilon_{Nd(i)}$ =					**2 %**	**25 %**	**11.92 %**	**0.41**	**-15 to -10**
-16 to -11					**3 %**	**28 %**	**11.86 %**	**0.34**	**-20 to -13**
					4 %	**30 %**	**12.60 %**	**0.45**	**-23 to -15**
					5 %	*31 %*	*14.18 %*	*0.69*	*-25 to -17*
					6 %	*33 %*	*16.12 %*	*0.95*	*-27 to -18*
					7 %	*34 %*	*17.60 %*	*1.19*	*-28 to -19*
					8 %	*36 %*	*19.40 %*	*1.43*	*-30 to -20*
					9 %	*37 %*	*21.06 %*	*1.68*	*-30 to -21*
					10 %	*39 %*	*22.61 %*	*1.93*	*-31 to -21*
	EC-AFC	Archean TTG	PM_{CT}	0.5	*1 %*	*22 %*	*30.92 %*	*2.21*	*+4 to +5*
					2 %	*25 %*	*28.00 %*	*1.79*	*0 to +2*
					3 %	*28 %*	*25.47 %*	*1.46*	*-3 to 0*
					4 %	*30 %*	*23.24 %*	*1.21*	*-5 to -2*
					5 %	*31 %*	*20.78 %*	*0.97*	*-7 to -3*
					6 %	*33 %*	*18.61 %*	*0.79*	*-9 to -5*
					7 %	*34 %*	*16.82 %*	*0.66*	*-11 to -6*
					8 %	*36 %*	*15.01 %*	*0.55*	*-13 to -7*
					9 %	*37 %*	*13.19 %*	*0.47*	*-14 to -9*
					10 %	*39 %*	*11.88 %*	*0.40*	*-16 to -10*
					11 %	**40 %**	**11.72 %**	**0.37**	**-17 to -10**
					12 %	**41 %**	**11.74 %**	**0.34**	**-17 to -11**
					13 %	**42 %**	**11.79 %**	**0.33**	**-19 to -12**
					14 %	**43 %**	**11.82 %**	**0.33**	**-20 to -13**
					15 %	**44 %**	**11.86 %**	**0.34**	**-20 to -13**
					16 %	*46 %*	*12.02 %*	*0.36*	*-21 to -14*
					17 %	*46 %*	*12.18 %*	*0.38*	*-22 to -14*
					18 %	*47 %*	*12.40 %*	*0.42*	*-22 to -15*
					19 %	*49 %*	*12.62 %*	*0.46*	*-23 to -15*

					20 %	*49 %*	*12.85 %*	*0.49*	*-24 to -16*
CT2	AFC	SCLM1	PM_{CT}	-	**1 %**	**13 %**	**8.98 %**	**0.27**	**-1 to +4**
$\varepsilon_{Nd(i)}$ =					**2 %**	**27 %**	**16.04 %**	**0.98**	**-5 to +2**
-7 to 0					**3 %**	**40 %**	**25.32 %**	**2.59**	**-8 to +1**
					4 %	*53 %*	*34.15 %*	*4.63*	*-10 to 0*
					5 %	*67 %*	*42.66 %*	*6.85*	*-12 to -1*
	AFC	SCLM1	PM_{LN}	-	**1 %**	**13 %**	**7.43 %**	**0.17**	**+2 to +5**
					2 %	**27 %**	**8.24 %**	**0.18**	**-2 to +4**
					3 %	**40 %**	**15.75 %**	**0.73**	**-5 to +2**
					4 %	*53 %*	*23.17 %*	*1.62*	*-7 to +1*
					5 %	*67 %*	*29.76 %*	*2.74*	*-8 to +1*
CT3	AFC	SCLM2	PM_{CT}	-	*1 %*	*4 %*	*13.86 %*	*0.44*	*+7 to +8*
$\varepsilon_{Nd(i)}$ =					*2 %*	*8 %*	*11.90 %*	*0.32*	*+6 to +7*
-2 to +2					*3 %*	*12 %*	*10.02 %*	*0.22*	*+5 to +7*
					4 %	*16 %*	*8.21 %*	*0.16*	*+4 to +6*
					5 %	*20 %*	*6.75 %*	*0.11*	*+3 to +6*
					6 %	**24 %**	**5.92 %**	**0.08**	**+2 to +5**
					7 %	**28 %**	**5.12 %**	**0.08**	**+1 to +5**
					8 %	**32 %**	**4.62 %**	**0.08**	**0 to +4**
					9 %	**36 %**	**4.58 %**	**0.10**	**-1 to +4**
					10 %	**40 %**	**5.19 %**	**0.14**	**-1 to +4**
					11 %	*44 %*	*6.01 %*	*0.18*	*-2 to +4*
					12 %	*48 %*	*6.84 %*	*0.24*	*-2 to +3*
					13 %	*52 %*	*7.80 %*	*0.30*	*-3 to +3*
					14 %	*56 %*	*9.00 %*	*0.37*	*-4 to +3*
					15 %	*60 %*	*10.17 %*	*0.45*	*-4 to +3*

Best-fit results shown in Figs. 7–10 are shown in bold.

PM = Parental melt (see Tables 1 and 2). $\mathbf{D_c(x)}$ = Partition coefficient for all of the elements in the crustal contaminant. $\mathbf{M_a}$ = Mass of the assimilated material relative to mass of the original melt. $\mathbf{M_c}$ = Mass of crystallized material relative to the mass of the original melt. $\mathbf{error_{avg}\ (Sm_{NN} = 1)}$ = Average error of double-normalized (first to primitive mantle, then to primitive-mantle-normalized average magma type composition (calculated on the basis of representative samples) so that model $Sm_{NN} = 1$) trace element pattern of the model result relative to that of the average magma type. Calculated as an average of errors of all the elements, for Sm the error is 0%. $\mathbf{residuals^2\ (Sm_{NN} = 1)}$ = Squared residuals of the double-normalized model results relative to the average magma type trace element pattern, for Sm residual is 0.

Heinonen, J.S., Luttinen, A.V., Bohrson, W.A. 2016. Enriched continental flood basalts from depleted mantle melts: modeling the lithospheric contamination of Karoo lavas from Antarctica. Contributions to Mineralogy and Petrology 171:9. http://dx.doi.org/10.1007/s00410-015-1214-8 (Author's postprint)

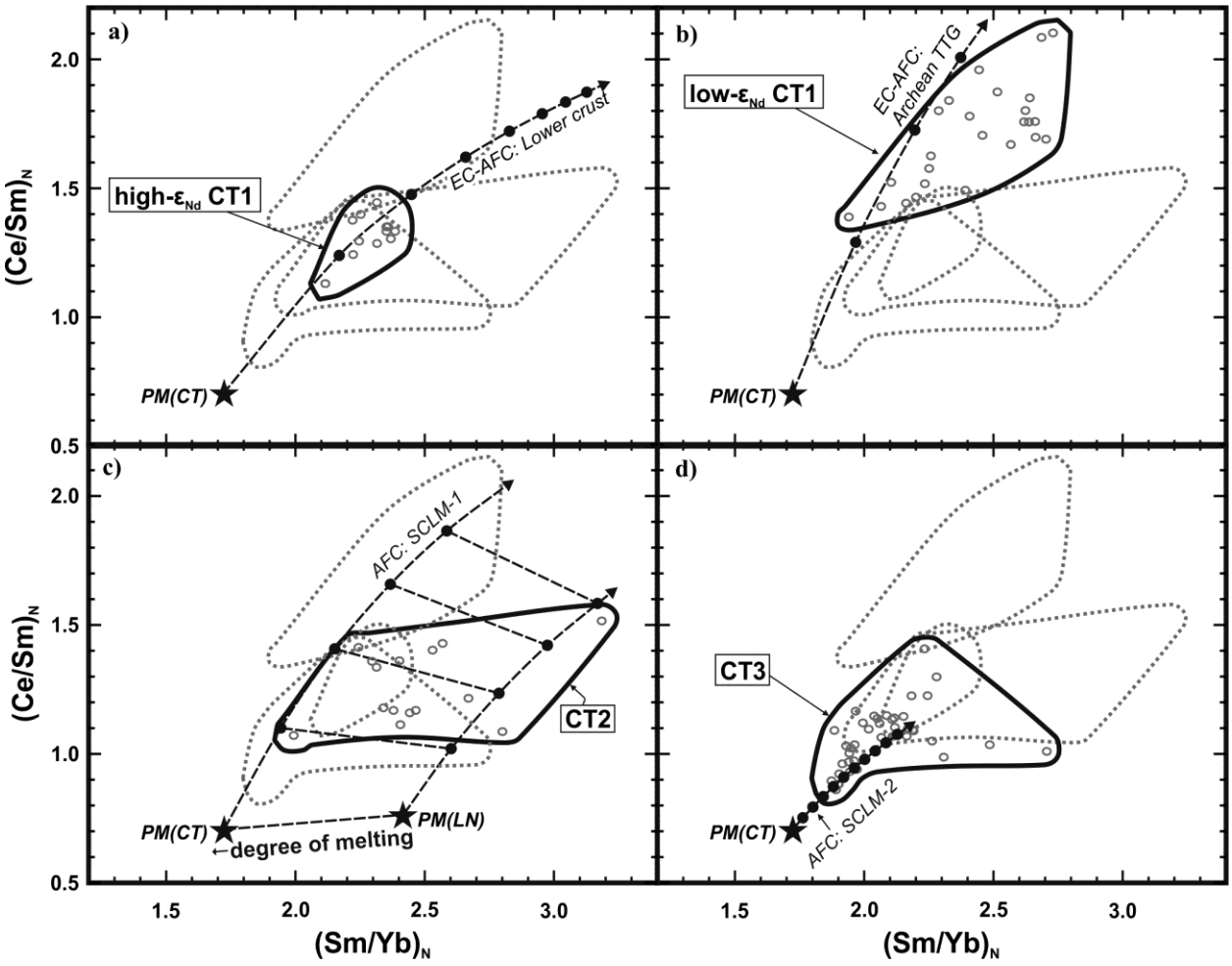

Fig. 11. Chondrite-normalized (McDonough and Sun, 1995) Sm/Yb vs. Ce/Sm for the different CT magma types and contamination models (Figs. 7–10). Filled circles have been drawn in intervals that represent 1% of contamination relative to the original parental melt (PM_{CT} or PM_{LN}). Only EC-AFC models with $D_c(x) = 0.1$ are shown for clarity in a) and b); models with $D_c(x) = 0.5$ would roughly follow the same trajectories, but show higher degree of contamination at a given Sm/Yb or Ce/Sm.

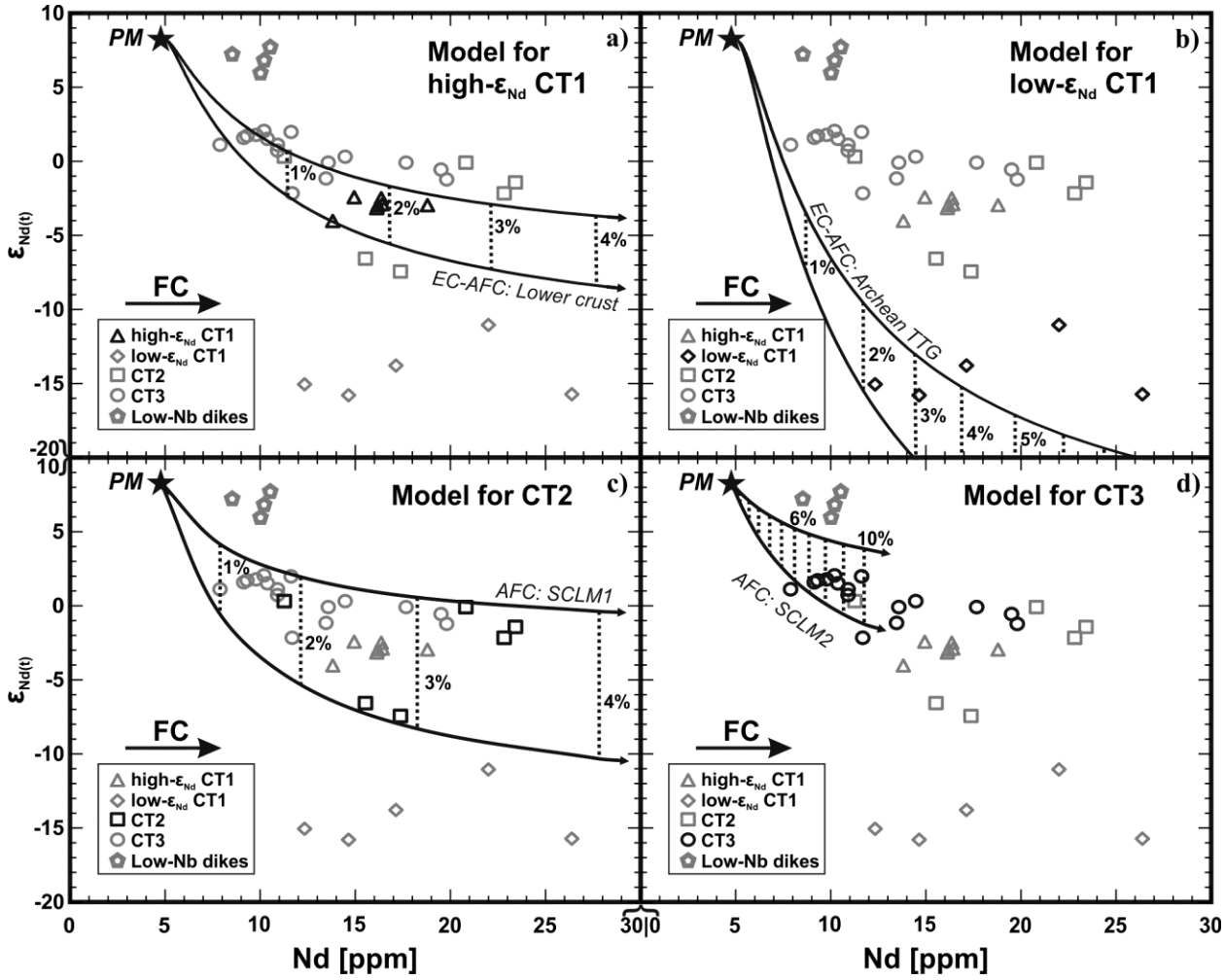

Fig. 12. Nd [ppm] vs. $\varepsilon_{Nd(t)}$ for the Low-Nb dikes, Vestfjella CT magma types (different groups highlighted in insets), and respective EC-AFC and AFC contamination models (Table 2). The two separate model lines represent the isotopic variation of the contaminants (Table 2; $\varepsilon_{Nd(t)}$ from -13 to -7 assumed for the lower crustal contaminant, see text) and the vertical stippled lines indicate the amount of contamination relative to the original parental melt (PM_{CT}). Only EC-AFC models with $D_c(x) = 0.1$ are shown for clarity in a) and b); models with $D_c(x) = 0.5$ would broadly follow the same trajectories, but show higher degree of contamination at a given Nd or ε_{Nd}. Models using PM_{LN} are not shown for CT2, but they would not be drastically different from the models using PM_{CT} in this case, although would begin at a higher Nd content (7.9 ppm). FC indicates fractional crystallization.

Discussion

Limitations of the presented models

Our modeling of the highly diverse CFB succession of Vestfjella involves numerous simplifications, e.g. regarding the compositional variability of the different magma types. In reality, each magma type, including the DM-sourced parental Low-Nb type, exhibit some variations in incompatible trace element and isotopic ratios (Figs. 5 and 12; Luttinen and Furnes 2000). Such variations cannot be explained by a simple two-component model. Technically, the presented models are also limited by uncertainties related to parameters required for modeling the partial melting of the lithospheric rock types.

The convergence of the geochemical trends of the lavas in, e.g., Sm/Yb vs. Ce/Sm space (Fig. 5), is compatible with a hypothesis of broadly similar DM-sourced parental magma compositions for the different magma types with some variance in the degree of source melting. Nevertheless, earlier studies have suggested that the sublithospheric sources of the Antarctic CFBs are heterogeneous by entraining recycled components (Heinonen et al. 2010; 2014) and being variably enriched in large-ion lithophile elements (Luttinen and Furnes 2000). Partial melting processes in such heterogeneous mantle and melting of heterogeneous wall-rocks during the ascent of the magmas likely produced variability in Vestfjella CFB magma compositions as well. The magmas were also likely to evolve within dynamic magma chambers that were characterized by refilling and mixing of distinct magma batches, similar to reported for CFBs of North Atlantic Igneous Province (Fowler et al. 2004). Consequently, the observed chemical trends represent overlapping of several unique liquid lines of descent, i.e. they reveal tendencies of differentiation processes. In the case of CT2 and CT3, assimilation may have taken place in the deep SCLM before significant fractionation of the magma (Fig. 13), and thus the selected r values (r = rate of assimilation divided by rate of fractional crystallization) for the respective AFC models should not be considered definitive (Table 2). Overall, we consider the variations in the source and wallrock composition, degree and pressure of melting, and differentiation processes to be of second-order importance and regard that possible fine-tunings of the best-fit models would not significantly strengthen or weaken the main arguments.

It is important to note that the presented EC-AFC models have equilibration temperatures close to the wallrock solidus and incorporate all partial melts from the wallrock to the magma (Table 2), and SCLM contaminants (i.e. lamproites and ijolites; Table 2) used in the AFC models represent relatively low degrees of SCLM melting. The degrees of contamination suggested by the AFC models and EC-AFC models with $D_c(x) = 0.1$ (Fig. 7–10; Table 3) may thus be considered to correspond to near-minimum estimates. Importantly, the limited variation in major element composition of the Vestfjella CFBs (Luttinen and Furnes 2000) indicates that mixing with compositionally anomalous components (e.g., Si-rich crust) cannot have been volumetrically significant. For example, if the slightly higher SiO_2 contents of the low-ε_{Nd} CT1 lavas (52.6 wt. % at MgO = 8 wt. %) compared to MORB-like dikes (50.5 wt. % at MgO = 8 wt. %) are attributed only to crustal contamination of the former, the input of Archean TTG material would be ~9 wt. % (assuming leucosome, i.e., TTG partial melt composition, SiO_2 = 74 wt. %; Kreissig et al. 2000). Such calculations are compatible with our trace element and isotopic modeling (Fig. 8) and provide support for the presented contamination scenarios.

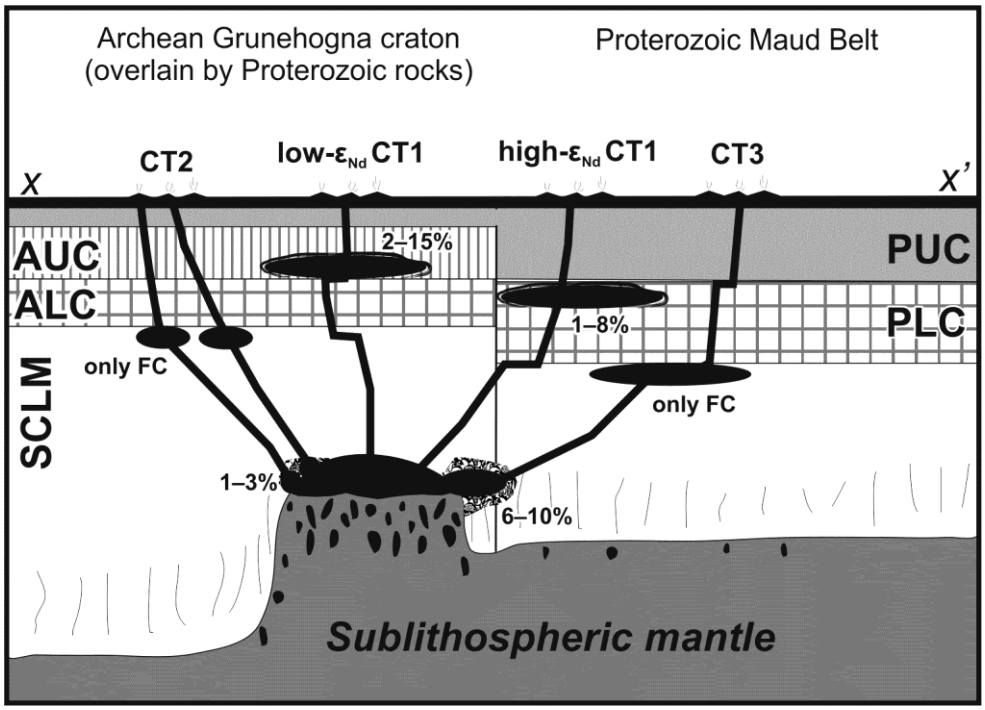

Fig. 13. A schematic cross-section across line segment x–x' (Figs. 1–2) during Karoo CFB magmatism with percentages indicating the degrees of lithospheric contamination (relative to the mass of the parental magma) required for the generation of each Vestfjella CFB magma type as suggested by our modeling (Fig. 7). Primary magma source (85–99% of the Vestfjella CFB material, depending on the magma type) is the sublithospheric mantle (black blobs represent partial melts). If CT2 and CT3 magmas avoided crustal contamination as suggested by the modeling, the fractionation (RTF) of the magmas may have taken place in magma chambers in refractory SCLM just below the Moho. AUC = Archean upper crust; ALC = Archean lower crust; PUC = Proterozoic upper crust; PLC = Proterozoic lower crust; SCLM = Subcontinental lithospheric mantle with metasomatized (veined) portions.

Implications

The key result of the presented modeling is that the diversification of relatively uniform DM-sourced magmas, akin to those sampled by the low-Nb dike suite, by incorporation of minor quantities of highly enriched partial melts from Gondwanan lithospheric mantle and crust can provide a geologically sound and geochemically and thermodynamically feasible petrogenetic explanation for the diagnostic compositional features of the Vestfjella CFBs (Fig. 13).

The implications of this finding range from local to global: mixing processes in a natural magma system are very likely to generate diverse compositions between the end-members. Grouping of the Vestfjella CFBs into distinctive chemical types strongly argues for effective homogenization of variably contaminated magma batches prior to eruption. Bearing in mind the scale and long duration (up to >5 Ma; Luttinen et al. 2015) of the voluminous low-ε_{Nd} CT1 and CT3 eruptions in Vestfjella, these magma types have probably been tapped from distinct long-lived and relatively large magma chambers. The quasi steady-state compositions of the lavas (Luttinen and Furnes 2000) are compatible with a RTF-type (periodically replenished and tapped, continuously fractionating; O'Hara and Mathews 1981; see Cox 1972) system that can

effectively buffer the compositions of magmas generated by mixing of highly contrasting components.

On the scale of the Karoo province, our modelling supports the view that DM-sources may have been significant despite the rarity and crosscutting relation of MORB-affinity rock types relative to the CFB lavas (see also Fig. 3b). More than ~90 wt. % of the Vestfjella CFB magmas have likely been derived from this DM-like mantle source (Fig. 13). High-precision trace element data are sparse for the low-Ti CFBs at the conjugate African margin (Fig. 1), but preliminary comparisons indicate similarity between the southern rift-assemblage basalt sequences of the Lebombo Monocline and low-ε_{Nd} CT1 (and CT2) (Luttinen and Furnes 2000). It is conceivable if not probable that models similar to those presented here could be successfully applied to the southern Lebombo CFBs. Importantly, previous geochemical models of the high-Ti rift-assemblage basalts and picrites (Ellam and Cox 1991; Luttinen et al. 2015) have envisaged a similar MORB-lamproite mixing process as we have proposed for the Vestfjella CT3 lavas. It must be emphasized that the geochemically different plateau-assemblage CFBs found outside the central rift zone were probably generated within different magma systems (Fig. 1; e.g., Duncan et al. 1984; Jourdan et al. 2007a; Luttinen et al. 2010, 2015; Neumann et al. 2011) and our models are not directly applicable to them. The chondritic Sm/Yb of the plateau-assemblage CFBs are indicative of magma generation at low pressures and it is difficult to constrain the feasible parental magma compositions due to lack of Mg-rich and high-$\varepsilon_{Nd(t)}$ lava compositions.

On a global scale, the presented models suggest that the importance of lithospheric CFB magma sources may have been overestimated in many CFB provinces (see also, e.g., Ewart et al. 2004; Kieffer et al. 2004): a CFB geochemical signature with strong lithospheric affinity is not necessarily a strong argument for a predominantly lithospheric magma source (Figs. 7–10). The models provide numerical support for the view that convective mantle is the principal magma source of terrestrial mafic magmatism in continental settings (Arndt and Christensen 1992; Arndt et al. 1993; Anderson 1994) and that CFBs represent major juvenile crustal growth events rather than just recycling of old lithospheric materials. Low-degree melting of crustal contaminants, as suggested by the modeling, could also explain the general rarity of coeval felsic volcanic rocks in CFB provinces.

At Vestfjella, the primitive uncontaminated MORB-like dikes provide key constraints for asthenospheric parental melt compositions (Fig. 6), but they comprise only a tiny portion of the well-exposed CFB successions. Their presence was revealed only after detailed mapping of the extremely well-exposed outcrops of Vestfjella during several Antarctic expeditions. Weathering, thick soil cover, and vegetation may hamper the discovery of such rare rock types and construction of contamination models in many other CFB provinces. The general applicability of high-pressure MORB- or oceanic island basalt-like parental melts and EC-AFC and AFC modeling in explaining the geochemical characteristics of "lithosphere-signatured" CFBs in detail remains to be tested, but the presented example from the Vestfjella mountain range provides a good basis for further research on this matter. Any such models should be based on characteristic trace elements patterns and isotopic compositions (Figs. 7–10; Table 3), not only on few selected trace element ratios.

Conclusions

Our case study on Karoo CFBs from Vestfjella, Antarctica, suggests that the longstanding thermodynamic ambiguities related to melting tens of percent of bulk crust or mantle lithosphere to produce CFB geochemical characteristics may be solved by using 1) EC-AFC equations for modeling of crustal contamination, 2) fertile SCLM partial melt compositions as contaminants in AFC modeling, and 3) reasonable estimates of asthenosphere-derived melts as parental magma compositions. Our calculations show that most of the geochemically diverse Vestfjella CFB magma types can be produced by just minor (1–15%) contamination of a depleted high-Mg parental magma, constrained on the basis of rare MORB-affinity dikes found in the area, with local or representative lithospheric components. Our modeling implies that CFBs may represent major juvenile crust forming events rather than recycling of lithospheric materials.

Acknowledgements

We greatly appreciate the comments of an anonymous reviewer and Fred Jourdan, and the editorial handling of the manuscript by Timothy Grove. We are especially grateful to the anonymous reviewer for pointing out the work of Harmer (1999) on alkaline rocks in southern Africa and for suggesting better ways for quantitative evaluation of the models. In addition, comments by J. Brendan Murphy, Andrew Kerr, Bill Leeman, and an anonymous reviewer on an earlier draft of the manuscript are appreciated and helped us to provide a more detailed treatment on the subject. Aku Heinonen and David Whipp are also thanked for out-of-the-box comments and suggestions that improved the manuscript. Frank Spera is acknowledged for general support of the collaboration that resulted in writing this manuscript. Some of the diagrams have been produced with the help of the GCDkit software (Janoušek et al., 2006). Our research is funded by the Academy of Finland (Grant no. 252652).

References

Adam J, Green TH (2006) Trace element partitioning between mica- and amphibole-bearing garnet lherzolite and hydrous basanitic melt: 1, Experimental results and the investigation of controls on partitioning behaviour. Contrib Mineral Petrol 152:1–17. doi:10.1007/s00410-006-0085-4

Anderson DL (1994) The sublithospheric mantle as the source of continental flood basalts: the case against the continental lithosphere and plume head reservoirs. Earth Planet Sci Lett 123:269–280. doi:10.1016/0012-821x(94)90273-9

Antonini P, Piccirillo EM, Petrini R, Civetta L, D'Antonio M, Orsi G (1999) Enriched mantle – Dupal signature in the genesis of the Jurassic Ferrar Tholeiites from Prince Albert Mountains (Victoria Land, Antarctica). Contrib Mineral Petrol 136:1–19. doi:10.1007/s004100050520

Arndt NT, Christensen U (1992) The role of lithospheric mantle in continental flood volcanism: Thermal and geochemical constraints. Journal of Geophysical Research: Solid Earth 97:10967–10981. doi:10.1029/92JB00564

Arndt NT, Czamanske GK, Wooden JL, Fedorenko VA (1993) Mantle and crustal contributions to continental flood volcanism. Tectonophysics 223:39–52. doi:10.1016/0040-1951(93)90156-e

Bea F (1996) Controls on the trace element composition of crustal melts. Trans R Soc Edinb Earth Sci 87:33–41. doi:10.1017/S0263593300006453

Bergman SC (1987) Lamproites and other potassium-rich igneous rocks: a review of their occurrence, mineralogy and geochemistry. In: Fitton JG, Upton BGJ (eds) Alkaline Igneous Rocks. Geol Soc London Spec Publ, vol 30, pp 103–190. doi:10.1144/GSL.SP.1987.030.01.08

Black BA, Lamarque J, Shields CA, Elkins-Tanton LT, Kiehl JT (2014) Acid rain and ozone depletion from pulsed Siberian Traps magmatism. Geology 42:67–70. doi:10.1130/G34875.1

Bohrson WA, Spera FJ (2001) Energy-constrained open-system magmatic processes II: Application of energy-constrained assimilation-fractional crystallization (EC-AFC) model to magmatic systems. J Petrol 42:1019–1041. doi:10.1093/petrology/42.5.1019

Bohrson WA, Spera FJ (2003) Energy-constrained open-system magmatic processes IV: Geochemical, thermal and mass consequences of energy-constrained recharge, assimilation and fractional crystallization (EC-RAFC). Geochem Geophys Geosyst 4. doi:10.1029/2002GC000316

Boudreau AE (1999) PELE – a version of the MELTS software program for the PC platform. Comput Geosci 25:201–203. doi:10.1016/s0098-3004(98)00117-4

Carlson RW, Lugmair GW, MacDougall JD (1981) Columbia River volcanism; the question of mantle heterogeneity or crustal contamination. Geochim Cosmochim Acta 45:2483–2499. doi:10.1016/0016-7037(81)90100-9

Chakhmouradian AR (2006) High-field-strength elements in carbonatitic rocks: Geochemistry, crystal chemistry and significance for constraining the sources of carbonatites. Chem Geol 235:138–160. doi:10.1016/j.chemgeo.2006.06.008

Chapman DS (1986) Thermal gradients in the continental crust. In: Dawson JB, Carlswell DA, Hall J, Wedepohl KH (eds) The Nature of the Lower Continental Crust. Geol Soc London Spec Publ, vol 24, pp 63–70. doi:10.1144/GSL.SP.1986.024.01.07

Corner B (1994) Geological evolution of western Dronning Maud Land within a Gondwana framework: Geophysics subprogramme. Final project report to SACAR. Department of Geophysics, Witwaterstrand University, South Africa, 21 p.

Cox KG (1972) The Karroo volcanic cycle. J Geol Soc 128:311–336. doi:10.1144/gsjgs.128.4.0311

Cox KG (1980) A model for flood basalt vulcanism. J Petrol 21:629–650. doi:10.1093/petrology/21.4.629

Cox KG (1988) The Karoo province. In: MacDougall JD (ed) Continental flood basalts. Kluwer Academic Publishers, Dordrecht, pp 239–271. doi:10.1007/978-94-015-7805-9_7

DePaolo DJ (1981a) Neodymium isotopes in the Colorado Front Range and crust-mantle evolution in the Proterozoic. Nature 291:193–196. doi:10.1038/291193a0

DePaolo DJ (1981b) Trace element and isotopic effects of combined wallrock assimilation and fractional crystallization. Earth Planet Sci Lett 53:189–202. doi:10.1016/0012-821x(81)90153-9

Duncan AR, Erlank AJ, Marsh JS (1984) Regional geochemistry of the Karoo igneous province. In: Erlank AJ (ed) Petrogenesis of the volcanic rocks of the Karoo Province, Geol Soc S Africa Spec Pub, vol 13, Johannesburg, South Africa, pp 355–388

Ellam RM (2006) New constraints on the petrogenesis of the Nuanetsi picrite basalts from Pb and Hf isotope data. Earth Planet Sci Lett 245:153–161. doi:10.1016/j.epsl.2006.03.004

Ellam RM, Cox KG (1989) A Proterozoic lithospheric source for Karoo magmatism: evidence from the Nuanetsi picrites. Earth Planet Sci Lett 92:207–218. doi:10.1016/0012-821X(89)90047-2

Ellam RM, Cox KG (1991) An interpretation of Karoo picrite basalts in terms of interaction between asthenospheric magmas and the mantle lithosphere. Earth Planet Sci Lett 105:330–342. doi:10.1016/0012-821X(91)90141-4

Ewart A, Milner SC, Armstrong RA, Duncan AR (1998) Etendeka volcanism of the Goboboseb Mountains and Messum igneous complex, Namibia. Part I: Geochemical evidence of Early Cretaceous Tristan plume melts and the role of crustal contamination in the Paraná-Etendeka CFB. J Petrol 39:191–225

Ewart A, Marsh JS, Milner SC, Duncan AR, Kamber BS, Armstrong RA (2004) Petrology and Geochemistry of Early Cretaceous Bimodal Continental Flood Volcanism of the NW Etendeka, Namibia. Part 1: Introduction, Mafic Lavas and Re-evaluation of Mantle Source Components. J Petrol 45:59–105. doi:10.1093/petrology/egg083

Farnetani CG, Richards MA, Ghiorso MS (1996) Petrological models of magma evolution and deep crustal structure beneath hotspots and flood basalt provinces. Earth Planet Sci Lett 143:81–94. doi:10.1016/0012-821X(96)00138-0

Fowler SJ, Bohrson WA, Spera FJ (2004) Magmatic Evolution of the Skye Igneous Centre, Western Scotland: Modelling of Assimilation, Recharge and Fractional Crystallization. J Petrol 45:2481–2505. doi:10.1093/petrology/egh074

Furnes H, Neumann E, Sundvoll B (1982) Petrology and geochemistry of Jurassic basalt dykes from Vestfjella, Dronning Maud Land, Antarctica. Lithos 15:295–304. doi:10.1016/0024-4937(82)90020-2

Furnes H, Vad E, Austrheim H, Mitchell JG, Garmann LB (1987) Geochemistry of basalt lavas from Vestfjella and adjacent areas, Dronning Maud Land, Antarctica. Lithos 20:337–356. doi:10.1016/0024-4937(87)90015-6

Gallagher K, Hawkesworth C (1992) Dehydration melting and the generation of continental flood basalts. Nature 358:57–59. doi:10.1038/358057a0

Ganino C, Arndt NT (2009) Climate changes caused by degassing of sediments during the emplacement of large igneous provinces. Geology 37:323–326. doi:10.1130/G25325A.1

Ghiorso MS, Sack RO (1995) Chemical mass transfer in magmatic processes IV. A revised and internally consistent thermodynamic model for the interpolation and extrapolation of liquid-solid equilibria in magmatic systems at elevated temperatures and pressures. Contrib Mineral Petrol 119:197–212. doi:10.1007/bf00307281

Gibson SA, Thompson RN, Dickin AP, Leonardos OH (1995) High-Ti and low-Ti mafic potassic magmas: Key to plume-lithosphere interactions and continental flood-basalt genesis. Earth Planet Sci Lett 136:149–165. doi:10.1016/0012-821X(95)00179-G

Goldstein SL, O'Nions RK, Hamilton PJ (1984) A Sm-Nd isotopic study of atmospheric dusts and particulates from major river systems. Earth Planet Sci Lett 70:221–236. doi:10.1016/0012-821X(84)90007-4

Grantham GH, Manhica ADST, Armstrong RA, Kruger FJ, Loubser M (2011) New SHRIMP, Rb/Sr and Sm/Nd isotope and whole rock chemical data from central Mozambique and western Dronning Maud Land, Antarctica: Implications for the nature of the eastern margin of the Kalahari Craton and the amalgamation of Gondwana. J Afr Earth Sci 59:74–100. doi:10.1016/j.jafrearsci.2010.08.005

Groenewald PB, Moyes AB, Grantham GH, Krynauw JR (1995) East Antarctic crustal evolution: geological constraints and modelling in western Dronning Maud Land. Precambrian Res 75:231–250. doi:10.1016/0301-9268(95)80008-6

Grosch EG, Bisnath A, Frimmel HE, Board WS (2007) Geochemistry and tectonic setting of mafic rocks in western Dronning Maud Land, East Antarctica: implications for the geodynamic evolution of the Proterozoic Maud Belt. J Geol Soc 164:465–475. doi:10.1144/0016-76492005-152

Harmer RE (1999) The petrogenetic association of carbonatite and alkaline magmatism: constraints from the Spitskop Complex, South Africa. J Petrol 40:525–548. doi:10.1093/petroj/40.4.525

Harmer RE, Lee CA, Eglington BM (1998) A deep mantle source for carbonatite magmatism: evidence from the nephelinites and carbonatites of the Buhera District, SE Zimbabwe. Earth Planet Sci Lett 158:131–142. doi:10.1016/s0012-821x(98)00053-3

Harris C, Marsh JS, Duncan AR, Erlank AJ (1990) The petrogenesis of the Kirwan Basalts of Dronning Maud Land, Antarctica. J Petrol 31:341–369. doi:10.1093/petrology/31.2.341

Harry DL, Leeman WP (1995) Partial melting of melt metasomatized subcontinental mantle and the magma source potential of the lower lithosphere. J Geophys Res B 100:10255–10269. doi:10.1029/94JB03065

Hawkesworth CJ, Marsh JS, Duncan AR, Erlank AJ, Norry MJ (1984) The role of continental lithosphere in the generation of the Karoo volcanic rocks: evidence from combined Nd- and Sr-isotope studies. In: Erlank AJ (ed) Petrogenesis of the volcanic rocks of the Karoo Province, Geol Soc S Africa Spec Pub, vol 13, Johannesburg, South Africa, pp 341–354

Heinonen JS, Luttinen AV (2008) Jurassic dikes of Vestfjella, western Dronning Maud Land, Antarctica: Geochemical tracing of ferropicrite sources. Lithos 105:347–364. doi:10.1016/j.lithos.2008.05.010

Heinonen JS, Luttinen AV (2010) Mineral chemical evidence for extremely magnesian subalkaline melts from the Antarctic extension of the Karoo large igneous province. Miner Petrol 99:201–217. doi:10.1007/s00710-010-0115-9

Heinonen JS, Carlson RW, Luttinen AV (2010) Isotopic (Sr, Nd, Pb, and Os) composition of highly magnesian dikes of Vestfjella, western Dronning Maud Land, Antarctica: A key to the origins of the Jurassic Karoo large igneous province? Chem Geol 277:227–244. doi:10.1016/j.chemgeo.2010.08.004

Heinonen JS, Carlson RW, Riley TR, Luttinen AV, Horan MF (2014) Subduction-modified oceanic crust mixed with a depleted mantle reservoir in the sources of the Karoo continental flood basalt province. Earth Planet Sci Lett 394:229–241. doi:10.1016/j.epsl.2014.03.012

Heinonen JS, Jennings ES, Riley TR (2015) Crystallisation temperatures of the most Mg-rich magmas of the Karoo LIP on the basis of Al-in-olivine thermometry. Chem Geol 411:26–35. doi:10.1016/j.chemgeo.2015.06.015

Hergt JM, Peate DW, Hawkesworth CJ (1991) The petrogenesis of Mesozoic Gondwana low-Ti flood basalts. Earth Planet Sci Lett 105:134–148. doi:10.1016/0012-821x(91)90126-3

Hersum TG, Marsh BD, Simon AC (2007) Contact Partial Melting of Granitic Country Rock, Melt Segregation, and Re-injection as Dikes into Ferrar Dolerite Sills, McMurdo Dry Valleys, Antarctica. J Petrol 48:2125–2148. doi:10.1093/petrology/egm054

Jacobs J, Thomas RJ, Weber K (1993) Accretion and indentation tectonics at the southern edge of the Kaapvaal craton during the Kibaran (Grenville) orogeny. Geology 21:203–206. doi:10.1130/0091-7613(1993)021<0203:AAITAT>2.3.CO;2

Jacobs J, Fanning CM, Henjes-Kunst F, Olesch M, Paech H (1998) Continuation of the Mozambique Belt into East Antarctica: Grenville-age metamorphism and polyphase Pan-African high-grade events in central Dronning Maud Land. J Geol 106:385–406. doi:10.1086/516031

Jacobs J, Fanning CM, Bauer W (2003) Timing of Grenville-age vs. Pan-African medium- to high grade metamorphism in western Dronning Maud Land (East Antarctica) and significance for correlations in Rodinia and Gondwana. Precambrian Res 125:1–20. doi:10.1016/S0301-9268(03)00048-2

Jacobs J, Pisarevsky S, Thomas RJ, Becker T (2008) The Kalahari Craton during the assembly and dispersal of Rodinia. Precambrian Res 160:142–158. doi:10.1016/j.precamres.2007.04.022

Janoušek V, Farrow CM, Erban V (2006) Interpretation of whole-rock geochemical data in igneous geochemistry: introducing Geochemical Data Toolkit (GCDkit). J Petrol 47:1255–1259. doi:10.1093/petrology/egl013

Jiang N, Carlson RW, Guo J (2011) Source of Mesozoic intermediate-felsic igneous rocks in the North China craton: Granulite xenolith evidence. Lithos 125:335–346. doi:10.1016/j.lithos.2011.02.017

Johnson TE, Gibson RL, Brown M, Buick IS, Cartwright I (2003) Partial Melting of Metapelitic Rocks Beneath the Bushveld Complex, South Africa. J Petrol 44:789–813. doi:10.1093/petrology/44.5.789

Jourdan F, Féraud G, Bertrand H, Kampunzu AB, Tshoso G, Watkeys MK, Le Gall B (2005) Karoo large igneous province: Brevity, origin, and relation to mass extinction questioned by new $^{40}Ar/^{39}Ar$ age data. Geology 33:745–748. doi:10.1130/G21632.1

Jourdan F, Bertrand H, Schaerer U, Blichert-Toft J, Féraud G, Kampunzu AB (2007a) Major and trace element and Sr, Nd, Hf, and Pb isotope compositions of the Karoo large igneous province, Botswana-Zimbabwe: lithosphere vs mantle plume contribution. J Petrol 48:1043–1077. doi:10.1093/petrology/egm010

Jourdan F, Féraud G, Bertrand H, Watkeys MK (2007b) From flood basalts to the inception of oceanization: example from the $^{40}Ar/^{39}Ar$ high-resolution picture of the Karoo large igneous province. Geochem Geophys Geosyst 8. doi:10.1029/2006GC001392

Kieffer B, Arndt N, Lapierre H, Bastien F, Bosch D, Pecher A, Yirgu G, Ayalew D, Weis D, Jerram DA, Keller F, Meugniot C (2004) Flood and Shield Basalts from Ethiopia: Magmas from the African Superswell. J Petrol 45:793–834. doi:10.1093/petrology/egg112

Kreissig K, Naegler TF, Kramers JD, van Reenen DD, Smit CA (2000) An isotopic and geochemical study of the northern Kaapvaal Craton and the Southern Marginal Zone of the Limpopo Belt: are they juxtaposed terranes? Lithos 50:1–25. doi:10.1016/S0024-4937(99)00037-7

Lana C, Reimold WU, Gibson RL, Koeberl C, Siegesmund S (2004) Nature of the archean midcrust in the core of the Vredefort dome, Central Kaapvaal Craton, South Africa. Geochim Cosmochim Acta 68:623–642. doi:10.1016/S0016-7037(03)00447-2

Larsen LM, Pedersen AK (2009) Petrology of the Paleocene Picrites and Flood Basalts on Disko and Nuussuaq, West Greenland. J Petrol 50:1667–1711. doi:10.1093/petrology/egp048

le Roex AP, Dick HJB, Erlank AJ, Reid AM, Frey FA, Hart SR (1983) Geochemistry, mineralogy and petrogenesis of lavas erupted along the Southwest Indian Ridge between the Bouvet triple junction and 11 degrees East. J Petrol 24:267–318. doi:10.1093/petrology/24.3.267

leRoex AP, Dick HJB, Watkins RT (1992) Petrogenesis of anomalous K-enriched MORB from the Southwest Indian Ridge: 11°53´E to 14°38´E. Contrib Mineral Petrol 110:253–268. doi:10.1007/BF00310742

Lightfoot PC, Hawkesworth CJ, Hergt JM, Naldrett AJ, Gorbachev NS, Fedorenko VA, Doherty W (1993) Remobilisation of the continental lithosphere by a mantle plume: major-, trace-element, and Sr-, Nd-, and Pb-isotope evidence from picritic and tholeiitic lavas of the Noril'sk District, Siberian Trap, Russia. Contrib Mineral Petrol 114:171–188. doi:10.1007/BF00307754

Lindström S (1995) Early Late Permian palynostratigraphy and palaeo-biogeography of Vestfjella, Dronning Maud Land, Antarctica. Rev Palaeobot Palynol 86:157–173. doi:10.1016/0034-6667(94)00104-R

Luttinen AV, Furnes H (2000) Flood basalts of Vestfjella: Jurassic magmatism across an Archaean-Proterozoic lithospheric boundary in Dronning Maud Land, Antarctica. J Petrol 41:1271–1305. doi:10.1093/petrology/41.8.1271

Luttinen AV, Siivola JU (1997) Geochemical characteristics of Mesozoic lavas and dikes from Vestfjella, Dronning Maud Land: recognition of three distinct chemical types. In: Ricci CA (ed) The Antarctic Region: Geological Evolution and Processes. Siena: Terra Antarctica Publications, Italy, pp 495–503

Luttinen AV, Rämö OT, Huhma H (1998) Neodymium and strontium isotopic and trace element composition of a Mesozoic CFB suite from Dronning Maud Land, Antarctica: Implications for lithosphere and asthenosphere contributions to Karoo magmatism. Geochim Cosmochim Acta 62:2701–2714. doi:10.1016/S0016-7037(98)00184-7

Luttinen AV, Zhang X, Foland KA (2002) 159 Ma Kjakebeinet lamproites (Dronning Maud Land, Antarctica) and their implications for Gondwana breakup processes. Geol Mag 139:525–539. doi:10.1017/S001675680200674X

Luttinen AV, Leat PT, Furnes H (2010) Björnnutane and Sembberget basalt lavas and the geochemical provinciality of Karoo magmatism in western Dronning Maud Land, Antarctica. J Volcanol Geotherm Res 198:1–18. doi:10.1016/j.jvolgeores.2010.07.011

Luttinen AV, Heinonen JS, Kurhila M, Jourdan F, Mänttäri I, Vuori S, Huhma H (2015) Depleted mantle-sourced CFB magmatism in the Jurassic Africa-Antarctica rift: petrology and $^{40}Ar/^{39}Ar$ and U/Pb chronology of the Vestfjella dyke swarm, Dronning Maud Land, Antarctica. J Petrol. 56:919–952. doi:10.1093/petrology/egv022

Mahoney JJ, le Roex AP, Peng Z, Fisher RL, Natland JH (1992) Southwestern limits of Indian Ocean ridge mantle and the origin of low $^{206}Pb/^{204}Pb$ mid-ocean ridge basalt: isotope systematics of the central Southwest Indian Ridge (17°–50°E). J Geophys Res 97:19771–19790. doi:10.1029/92JB01424

Marschall HR, Hawkesworth CJ, Storey CD, Dhuime B, Leat PT, Meyer H-, Tamm-Buckle S (2010) The Annandagstoppane Granite, East Antarctica: Evidence for Archaean Intracrustal recycling in the Kaapvaal-Grunehogna Craton from zircon O and Hf isotopes. J Petrol 51:2277–2301. doi:10.1093/petrology/egq057

McDonough WF, Sun SS (1995) The composition of the Earth. Chem Geol 120:223–253. doi:10.1016/0009-2541(94)00140-4

Menzies MA (1992) The lower lithosphere as a major source for continental flood basalts: a re-appraisal. In: Storey BC, Alabaster T, Pankhurst RJ (eds) Magmatism and the causes of continental break-up. Geol Soc London Spec Publ, vol 68, pp 31–39. doi:10.1144/gsl.sp.1992.068.01.03

Molzahn M, Reisberg L, Wörner G (1996) Os, Sr, Nd, Pb, O isotope and trace element data from the Ferrar flood basalts, Antarctica: evidence for an enriched subcontinental lithospheric source. Earth Planet Sci Lett 144:529–545. doi:10.1016/S0012-821X(96)00178-1

Moyes AB, Krynauw JR, Barton JM,Jr (1995) The age of the Ritscherflya Supergroup and Borgmassivet Intrusions, Dronning Maud Land, Antarctica. Antarct Sci 7:87–97. doi:10.1017/S0954102095000125

Nash WP, Crecraft HR (1985) Partition coefficients for trace elements in silicic magmas. Geochim Cosmochim Acta 49:2309–2322. doi:10.1016/0016-7037(85)90231-5

Neumann E, Svensen H, Galerne CY, Planke S (2011) Multistage Evolution of Dolerites in the Karoo Large Igneous Province, Central South Africa. J Petrol 52:959–984. doi:10.1093/petrology/egr011

O'Hara MJ, Mathews RE (1981) Geochemical evolution in an advancing, periodically replenished, periodically tapped, continuously fractionated magma chamber. J Geol Soc 138:237–277. doi:10.1144/gsjgs.138.3.0237

Perritt S (2001) The Ahlmannryggen Group, western Dronning Maud Land, Antarctica. PhD thesis, University of Natal, Durban, South Africa, 153 p.

Riley TR, Millar IL (2014) Geochemistry of the 1100 Ma intrusive rocks from the Ahlmannryggen region, Dronning Maud Land, Antarctica. Antarct Sci 26:389–399. doi:10.1017/S0954102013000916

Riley TR, Leat PT, Curtis ML, Millar IL, Duncan RA, Fazel A (2005) Early-middle Jurassic dolerite dykes from western Dronning Maud Land (Antarctica): identifying mantle sources in the Karoo Large Igneous Province. J Petrol 46:1489–1524. doi:10.1093/petrology/egi023

Riley TR, Curtis ML, Leat PT, Watkeys MK, Duncan RA, Millar IL, Owens WH (2006) Overlap of Karoo and Ferrar magma types in KwaZulu-Natal, South Africa. J Petrol 47:541–566. doi:10.1093/petrology/egi085

Rudnick RL, Gao S (2003) The Composition of the Continental Crust. In: Rudnick RL (ed) The Crust. Treatise on Geochemistry, vol 3, Elsevier-Pergamon, Oxford, pp 1–64. doi:10.1016/b0-08-043751-6/03016-4

Spera FJ, Bohrson WA (2001) Energy-constrained open-system magmatic processes I: General model and energy-constrained assimilation and fractional crystallization (EC-AFC) formulation. J Petrol 42:999–1018. doi:10.1093/petrology/42.5.999

Spera FJ, Bohrson WA (2002) Energy-constrained open-system magmatic processes 3. Energy-Constrained Recharge, Assimilation, and Fractional Crystallization (EC-RAFC). Geochem Geophys Geosyst 3. doi:10.1029/2002GC000315

Spera FJ, Bohrson WA (2004) Open-System Magma Chamber Evolution: an Energy-constrained Geochemical Model Incorporating the Effects of Concurrent Eruption, Recharge, Variable Assimilation and Fractional Crystallization (EC-E′RAχFC). J Petrol 45:2459–2480. doi:10.1093/petrology/egh072

Sun SS, McDonough WF (1989) Chemical and isotopic systematics of oceanic basalts: Implications for mantle composition and processes. In: Saunders AD, Norry MJ (eds) Magmatism in the ocean basins. Geol Soc London Spec Publ, vol 42, pp 313–345. doi:10.1144/GSL.SP.1989.042.01.19

Sweeney RJ, Falloon TJ, Green DH, Tatsumi Y (1991) The mantle origins of Karoo picrites. Earth Planet Sci Lett 107:256–271. doi:10.1016/0012-821x(91)90075-s

Sweeney RJ, Duncan AR, Erlank AJ (1994) Geochemistry and petrogenesis of central Lebombo basalts of the Karoo igneous province. J Petrol 35:95–125. doi:10.1093/petrology/35.1.95

Talarico F, Borsi L, Lombardo B (1995) Relict granulites in the Ross Orogen of northern Victoria Land (Antarctica), II. Geochemistry and palaeo-tectonic implications. Precambrian Res 75:157–174. doi:10.1016/0301-9268(95)80004-2

Thompson RN, Gibson SA (2000) Transient high temperatures in mantle plume heads inferred from magnesian olivines in Phanerozoic picrites. Nature 407:502–506. doi:10.1038/35035058

Vuori SK, Luttinen AV (2003) The Jurassic gabbroic intrusion of Utpostane and Muren: insights into Karoo-related plutonism in Dronning Maud Land, Antarctica. Antarct Sci 15:283–301. doi:10.1017/S0954102003001287

Wareham CD, Pankhurst RJ, Thomas RJ, Storey BC, Grantham GH, Jacobs J, Eglington BM (1998) Pb, Nd, and Sr Isotope Mapping of Grenville-Age Crustal Provinces in Rodinia. J Geol 106:647–660. doi:10.1086/516051

Will TM, Frimmel HE, Zeh A, Le Roux P, Schmädicke E (2010) Geochemical and isotopic constraints on the tectonic and crustal evolution of the Shackleton Range, East Antarctica, and correlation with other Gondwana crustal segments. Precambrian Res 180:85–112. doi:10.1016/j.precamres.2010.03.005

Workman RK, Hart SR (2005) Major and trace element composition of the depleted MORB mantle (DMM). Earth Planet Sci Lett 231:53–72. doi:10.1016/j.epsl.2004.12.005

Xu J, Suzuki K, Xu Y, Mei H, Li J (2007) Os, Pb, and Nd isotope geochemistry of the Permian Emeishan continental flood basalts: Insights into the source of a large igneous province. Geochim Cosmochim Acta 71:2104–2119. doi:10.1016/j.gca.2007.01.027

Ying J, Zhang H, Tang Y (2010) Lower crustal xenoliths from Junan, Shandong province and their bearing on the nature of the lower crust beneath the North China Craton. Lithos 119:363–376. doi:10.1016/j.lithos.2010.07.015

Yu J, Xu X, O'Reilly SY, Griffin WL, Zhang M (2003) Granulite xenoliths from Cenozoic Basalts in SE China provide geochemical fingerprints to distinguish lower crust terranes from the North and South China tectonic blocks. Lithos 67:77–102. doi:10.1016/S0024-4937(02)00253-0